SHORT TERM FORMATION OF THE INHIBITION LAYER DURING CONTINUOUS HOT-DIP GALVANIZING

SHORT TERM FORMATION OF THE INHIBITION LAYER DURING CONTINUOUS HOT-DIP GALVANIZING

By

LIHUA CHEN, B. E., M. Sc.

A Thesis

Submitted to the School of Graduate Studies

in Partial Fulfillment of the Requirements

For the Degree

Master of Applied Science

McMaster University

MASTER OF APPLIED SCIENCE (2006) McMaster University
(Materials Science & Engineering) Hamilton, Ontario

TITLE: Short Term Formation of the Inhibition Layer during Continuous Hot-Dip Galvanizing

AUTHOR: Lihua Chen, B. E., M. Sc. (China University of Geoscience, Beijing, China)
SUPERVISOR: Dr. Joseph. R. McDermid

NUMBER OF PAGES: xiv, 117

ABSTRACT

Aluminum is usually added to the zinc bath to form an Fe-Al interfacial layer which retards the formation of a series of Fe-Zn intermetallic compounds during the hot-dip galvanizing process. However, experimentally exploring the inhibition layer formation and obtaining useful experimental data to understand the mechanisms is quite challenging due to short times involved in this process. In this study, a galvanizing simulator was used to perform dipping times as short as 0.1s and rapid spot cooling techniques have been applied to stop the reaction between the molten zinc coating and steel substrate as quickly as possible. In addition, the actual reaction time has been precisely calculated through the logged sample time and temperature during the hot-dipping process. The kinetics and formation mechanism of the inhibition layer was characterized using SEM, ICP and EBSD based on the total reaction time. For bath containing 0.2wt% dissolved Al, the results show that $FeAl_3$ nucleates and grows during the initial stage of the inhibition layer formation and then Fe_2Al_5 forms by a diffusive transformation. The evolution of the interfacial layer formed in a zinc bath with 0.13wt% dissolved Al, including Fe-Al and Fe-Zn intermetallic compounds, was a result of competing reactions. In the initial period, the Fe-Al reaction dominated due to high thermodynamic driving forces. After the zinc concentration reached a critical composition in the substrate grain boundaries, formation of Fe-Zn intermetallic compounds was kinetically favoured. Fe-Zn intermetallic compounds formed due to zinc diffusing to the substrate via short circuit paths and continuously grew by consuming Fe-Al interfacial layer after samples exited the zinc

bath due to the limited Al supply. A mathematical model to describe the formation kinetics as a function of temperature for the 0.2wt% Al zinc bath was proposed. It indicated that the development of microstructure of the interfacial layer had significant influence on the effective diffusion coefficient and growth of this layer. However, the model underestimates the Al uptake by the interfacial layer, particularly at higher temperatures. This is thought to be due to the effect of the larger number of triple junctions in the inhibition layer leading to an underestimation of the effective diffusivity.

ACKNOWLEDGEMENTS

I would like to express my sincere gratitude to my supervisor, Dr. Joseph. R. McDermid, for his encouragement, scientific guidance, support and patience during the course of my study.

My gratitude is extended to: Jason Lavallée for his hard work to run a lot of steel panels in the galvanizing simulator; John Rodda and Doug Culley for their technical assistant in the use of ICP and preparing standard solutions; Steve Koprich for his professional assistant in obtaining SEM images; Florent Lefevre-Schlick for his friendly help and guidance in sample preparation and operations for EBSD; Chris Butcher for his assistant in use of microscopy.

Thanks also go to all members of our research group and friends in my office, Richard Fourmentin, Erika Bellhouse, Jinichiro Nakano, Xin Pang, Xuli Xia for their friendship and kindness.

My husband, Jianghua Li, and the rest of my family deserve special gratitude. Their spiritual support, love and understanding are invaluable. My little girl, Michelle Zihan Li, brings me a lot of laughter and happiness.

Grateful acknowledgement was given to Stelco Inc., the Natural Sciences and Engineering Research Council of Canada (NSERC) and the members of the McMaster Steel Research Centre for their financial support

TABLE OF CONTENTS

LIST OF FIGURES

Chapter 2

Chapter 5

LIST OF TABLES

Chapter 2

Chapter 3

Chapter 5

CHAPTER 1. INTRODUCTION

For over a century, zinc coatings have been used to provide corrosion protection to steels. Zinc coatings stop corrosion by providing two types of protection - a physical barrier and galvanic protection. Continuous hot-dip galvanizing is more advantageous than other galvanizing methods for steel sheet because it is a high-speed, low-cost, high volume process that controls not only the coating operation, but the strength and formability of the steel substrate via a pre-dipping anneal.

Aluminum is usually added to the zinc bath to form an Fe-Al intermetallic compound layer which retards the formation of a series of Fe-Zn intermetallic compounds and enhances the adhesion and formability of zinc coatings. For galvanizing researchers, understanding the Fe-Al interfacial layer formation mechanism is very important. A better understanding of the interfacial Fe-Al reactions might lead to better management of the galvanizing process and a better quality product. Some work has been done to investigate the microstructure, composition, formation mechanisms and reaction kinetics of this interfacial layer. However there is still considerable debate and discussion on this subject.

Basically, the reactions can be broken into three steps after the steel sheet enters a zinc bath containing Al: (1) dissolution of Fe from the steel surface into the zinc bath (2)

nucleation of the Fe-Al interfacial layer on the steel surface and (3) diffusion controlled growth of the interfacial layer. To the best of our current knowledge, these three reactions take place in seconds. In particular, the first two steps likely occur within one second.

Due to the short time scales involved, experimentally exploring each stage of inhibition layer formation and obtaining useful experimental data to understand the mechanisms is quite challenging. Some researchers [Toussaint *et al.*, 1998 (A)] claim that their data for immersion times as short as 0.1 second can be used to construct useful kinetic models of this process. However, they neglected the post-immersion diffusion of Al during coating solidification [Dubois, 2004] [Furdanowicz *et al.*, 1999] [Faderl *et al.*, 1995] which means that the reaction time between zinc overlay and substrate was underestimated and, thus, the "true" reaction time was not assessed.

Based on the above discussion, the present work undertakes to investigate the kinetics and mechanisms of Fe-Al interfacial layer formation using *actual* reaction times and to reduce the reaction times to as short as possible in order to determine the kinetics of the short-time reactions. In order to fulfill this purpose, the McMaster galvanizing simulator has been used to perform dipping times as short as 0.1s and the actual reaction time has been accurately calculated through the logged sample time and temperature during the hot-dipping process. In addition, rapid cooling techniques have been applied immediately after the steel sample was removed from the zinc pot to arrest the reaction between the steel substrate and zinc coating.

The work embodied in this thesis is presented in the following five chapters:

1. Theoretical considerations of reactions occurring during the continuous hot-dip galvanizing process and literature review are presented.
2. The development of the experimental apparatus, experimental parameters and analytical procedures are discussed.
3. Experimental results concerning the microstructure, surface roughness, kinetics, phase constitution and orientation of the inhibition layer using SEM, ICP, AFM and EBSD will be presented.
4. The kinetic mechanisms, reaction paths during the process of inhibition layer formation and a mathematical model based on the experimental results presented in the previous chapter will be discussed.
5. Conclusions will be drawn from this research work and recommendations are presented for future work

CHAPTER 2. LITERATURE REVIEW

2.1 Introduction

2.1.1 The Continuous Hot Dip Galvanizing Process

Due to its excellent corrosion protection, galvanized steel is used in thousands of applications throughout the world, especially in the construction, appliance and automotive industries. Hot dip zinc coating methods include batch galvanizing and continuous processing. The term continuous galvanizing is used for the coating of steel sheet in a process in which coils of steel are welded end-to-end and fed continuously through the coating facility. Continuous galvanizing may be either hot-dipped in molten Zn alloys or electrolytic. The term general galvanizing is used for an intermittent batch process in which steel work pieces are dipped in a molten bath of zinc.

The continuous galvanizing process has been in existence for over fifty years. Today, the manufacturing industry is using continuously hot-dip coated products for the most demanding applications that require not only a high surface quality, but also a high degree of formability. The most common type of continuous hot-dip coating processing line in use today consists of a series of steps, Figure 2-1, which may include the following sequential operations [Marder, 2000]:

• Coil welding to allow the process to be continuous

• Surface preparation: the steel sheets go through caustic cleaning and rinsing in order to remove rolling oils, dirt and iron fines

• Annealing in a N_2/H_2 reducing atmosphere to reduce surface Fe oxides and obtain the desired mechanical properties

• Application of the molten Zn (Al) coating to the steel surface

• Gas wiping to remove excess coating metal and obtain the desired coating thickness

• Cooling by forced air or additional processing to an inline heat treatment (galvannealing)

• Post-treatment: temper rolling, tension leveling, applying a coating of rust-inhibitive oil and recoiling

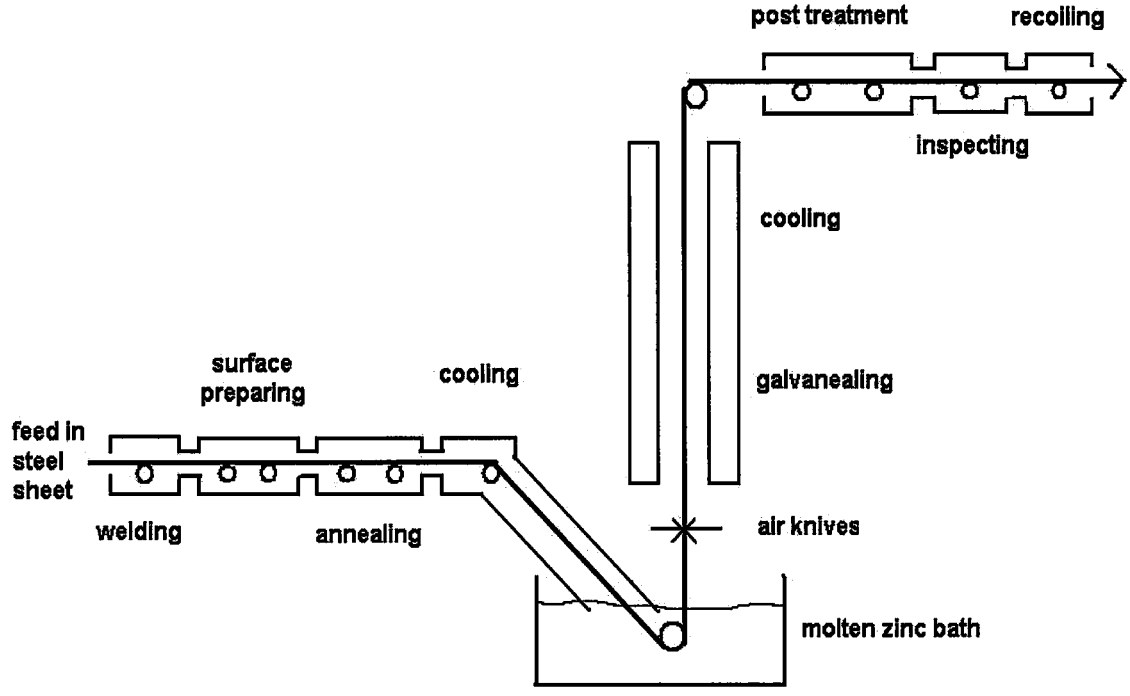

Figure 2-1: Schematic of continuous hot-dip galvanizing process [Marder, 2000]

2.1.2 Inhibition of Fe-Al Reactions by Al Bath Additions

Aluminum is the most important alloying element added to continuous hot-dip galvanizing baths. Uniform attack of the substrate occurring in an aluminum-free zinc bath leads to the formation of a three-phase alloy layer morphology containing gamma (Fe_3Zn_{10}), delta ($FeZn_{10}$) and zeta ($FeZn_{13}$) Fe-Zn phases, as shown in Figure 2-2, [Jordan *et al.*, 1997 (A)] [Gellings *et al.*, 1979] [Gellings *et al.*, 1980]. Unfortunately, these phases exhibit very poor ductility, i.e., they are very hard and brittle. When the user wants to form the steel sheet, there is a tendency for cracks to develop at the coating /substrate interface and the zinc coating to flake off.

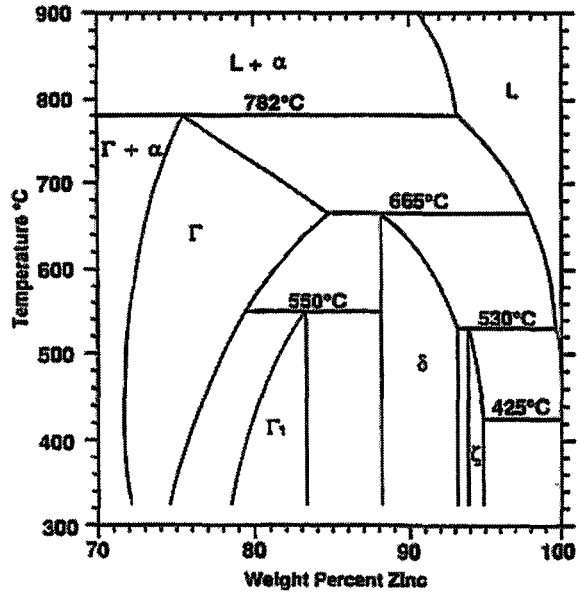

Figure 2-2: Zinc rich corner of the Fe-Zn binary phase diagram [Marder, 2000]

It is generally agreed that a small addition of Al in the zinc bath inhibits or retards Fe-Zn intermetallic formation between the zinc bath and iron substrate due to the formation of a

thin Fe-Al intermetallic layer at the Fe-Zn interface because aluminum has a greater affinity for iron than zinc, i.e. the formation free energy for Fe-Al intermetallic compounds is lower than that for Fe-Zn compounds [Marder, 2000] [Guttmann *et al.*, 1995].

Table 2-1 shows the characteristics of the Fe-Zn and Fe-Al intermetallic compounds frequently encountered in Zn-Al metallic coating. This Fe-Al interfacial layer improves the adhesion between the coating overlay and steel substrate, and allows the zinc overlay to remain ductile so that the steel sheet can be bent or shaped without compromising coating adhesion.

Table 2-1: Characteristics of selected Fe-Zn and Fe-Al intermetallic compounds [Guttmann, 1994]

Phase	Crystal Lattice	Fe (wt %) (450 °C)	ΔH* (450 °C) (kJ·mol^{-1})	ΔG* (450 °C) (kJ·mol^{-1})	HV
ζ ($FeZn_{13}$)	Monoclinic	5-6	-11.7	-2.8	112
δ ($FeZn_{10}$)	Hexagonal	7-12	-11.5	-3.5	340
Γ_1 (Fe_5Zn_{21})	FCC	17-19	-11.7	-4.1	326-496
Γ (Fe_3Zn_{10})	BCC	23-28	-10.9	-4.2	505
θ-$FeAl_3$	Monoclinic		-35.1	-30	
η-Fe_2Al_5	Orthorhombic		-34.6	-32	70

However, the inhibition of Fe-Zn reactions is always transient. Al inhibits the Fe-Zn reaction rather than suppressing it completely and after a certain reaction time, Fe-Zn intermetallic compounds appear [Jordan *et al.*, 1998; Jordan *et al.*, 1997 (B)]. Several mechanisms of inhibition layer breakdown have been proposed by galvanizing researchers. Some authors [Hisamatsu, 1989] [Guttmann *et al.*, 1995] [Lepretre *et al.*, 1998 (A)] explained inhibition layer breakdown as occurring via Zn diffusion through the short circuit diffusion paths in the Fe-Al interfacial layer (as shown in Figure 2-3), saturating the Fe substrate with Zn and resulting in Fe-Zn intermetallic compound formation. Guttmann *et al* [Guttmann, 1994] pointed out that random high angle boundaries of Fe_2Al_5 which are preferentially located at the grain boundaries of steel substrate are the short circuit diffusion path. However, other galvanizing researhers [Lin *et al.*, 1995 (A)] [Yamaguchi *et al.*, 1979] proposed Al depletion as the reason for the inhibition layer breakdown. Lin *et al* [Lin *et al.*, 1995 (A)] proposed a model concerning the transformation of the inhibition layer, in which the high concentration of Al in Fe-Al inhibition layer, which results in Al-depletion next to the inhibition layer, suppresses growth of the Fe-Al layer at the solid interfacial front. The growth of Fe-Zn-Al compounds continues by consuming the Zn-bearing Fe-Al interfacial layer and leads to the contact of the molten zinc bath with the steel substrate.

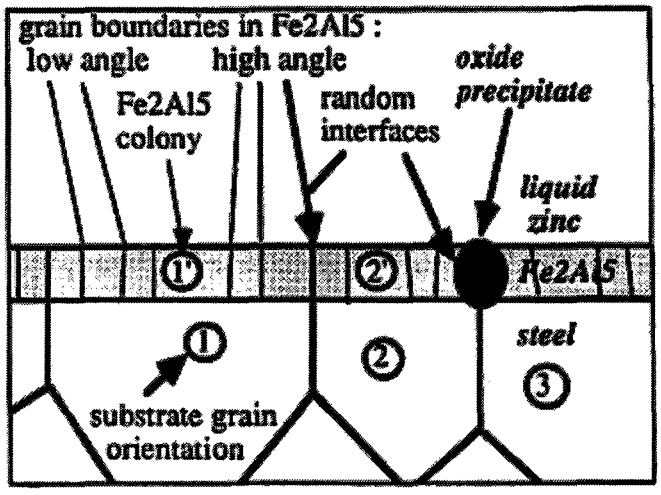

Figure 2-3: Short circuit Zn diffusion path through Fe_2Al_5 [Guttmann, 1994]

2.1.3 Reactions Occurring at the Interfacial Layer

The precise mechanisms of the reactions occuring between the steel and zinc bath are still a matter of debate, arising from three main factors, summarized as follows [Guttmann *et al.*, 1995] [Ebrill, 2000]:

(1) These reactions are complex, as they result from several intermingled steps: wetting of the solid substrate by liquid Zn, Fe dissolution from the substrate, isothermal solidification of Fe-Al-Zn intermetallic compounds, diffusional phase transformations in the solid phase and anisothermal solidification of Zn.

(2) The reactions are extremely rapid, as some of them take place in less than a second.

(3) The transformation front may often become unstable and thermodynamics cannot predict which phases actually appear, given the experimental conditions, as this is a matter of kinetics and not thermodynamic equilibrium [Philibert, 1994].

The galvanizing bath is essentially a chemical reactor and the three components Fe, Al, and Zn have different roles in this galvanizing reactor. As shown in the Figure 2-4, Fe is dissolved from the steel strip surface by the bath, which results in the formation of the inhibition layer and the formation of top and/or bottom intermetallic dross particles via Fe diffusion into the bath. Al can combine with Fe in the bulk bath to form η-Fe_2Al_5 particles, which eventually float to the bath surface to form top dross (a waste product) and Fe-Zn (principally $FeZn_{10}$) combine to form bottom dross (i.e. denser than liquid Zn bath) particles. Al also reacts with the Fe on the steel strip and deposit the Fe_2Al_5 phase or inhibition layer on the substrate, which inhibits the formation of Zn-Fe compounds [McDermid *et al.*, 2002 (A)] [Tang, 1998 (A)] [Tang, 1999]. Liquid zinc forms the bulk of the coating and dross.

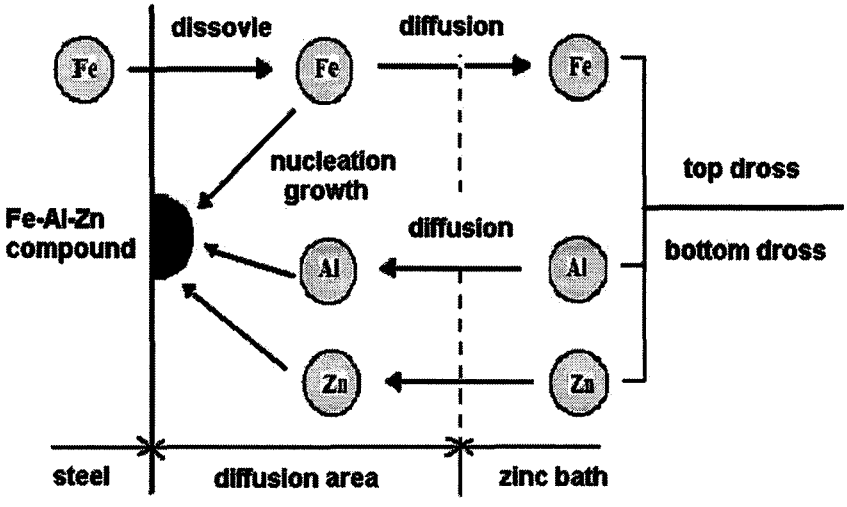

Figure 2-4: Schematic representation of galvanizing reactions [Giorgi *et al.*, 2004]

As the immersion time increases, the iron sheet continues to dissolve into the liquid zinc, due to the higher metastable Fe solubility in the vicinity of the strip/bath interface than that in the global equilibrium (as shown in Figure 2-5), which creates a local supersaturation of iron in the vicinity of the surface of the sheet. In consequence, as the equilibrium configuration of the zinc bath has to be finally satisfied, this supersaturation leads to the nucleation of Fe-Al or Fe-Zn intermetallic compound on the steel surface according to the aluminum content of the bath. These two steps can happen in a very short time and likely occur within one second. Price *et al* [Price *et al.*, 1999] revealed that the nucleation of the inhibition layer is extremely rapid, with a continuous layer formed within a 0.15 second immersion time by using SNMS and STRATA analysis software. Due to experimental difficulties, it is difficult to know how long the actual reaction time was. After the crystals of Fe-Al compound contact each other, the nucleation step is completed and is followed by diffusion controlled growth of the existing intermetallic layer.

It should be pointed out that, in the continuous galvanizing process, the transient chemistry in the vicinity of the strip/ Zinc interface deviates significantly from the bulk bath chemistry, and a thermodynamic equilibrium state is not always established [Tang, 1998 (A)]. Perrot *et al* [Perrot *et al.*, 1992] showed in their study related to the evolution with time of the Fe-Zn-Al diagram at 450 °C that short times, i.e. less than 30min, phase diagrams generally used by galvanizers is applicable, which is different from the stable

phase diagrams obtained when reaction times are longer than 1000 hours, as shown in Figure 2-6.

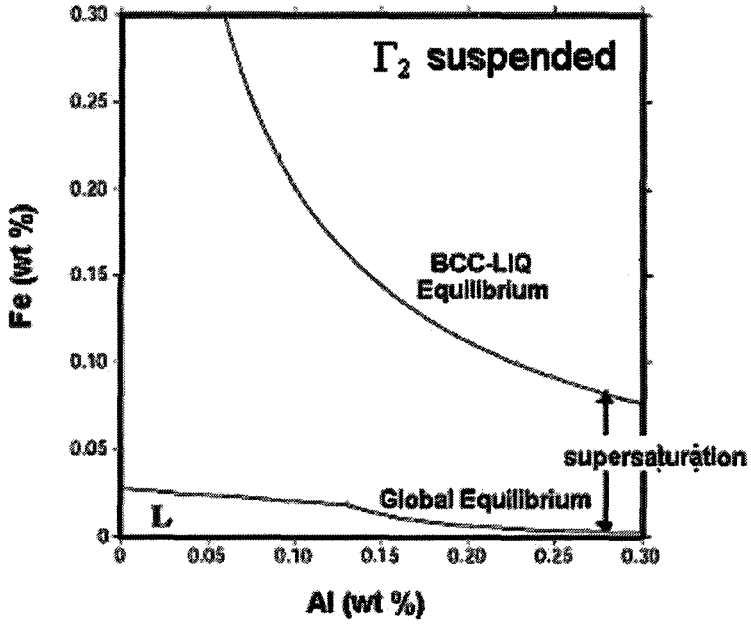

Figure 2-5: Potential supersaturation of the bath with iron at 450°C [Nakano, 2006]

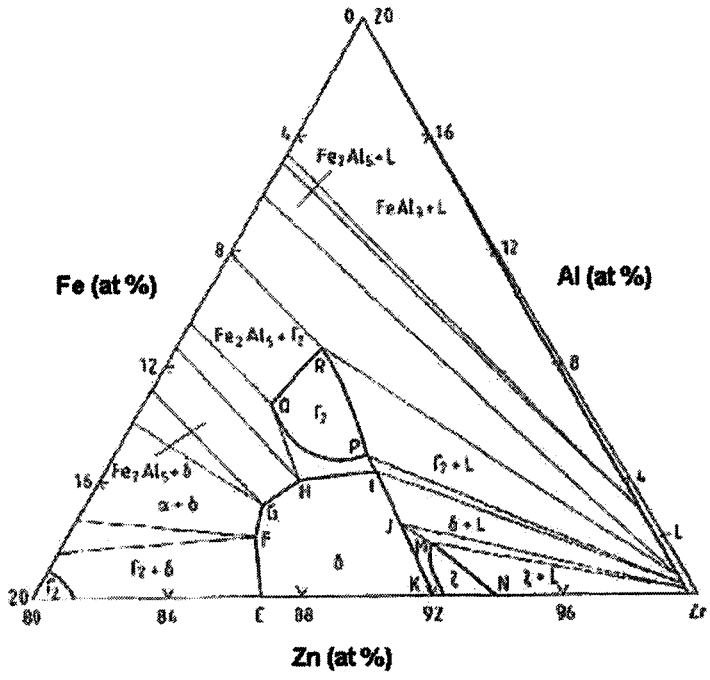

(a)

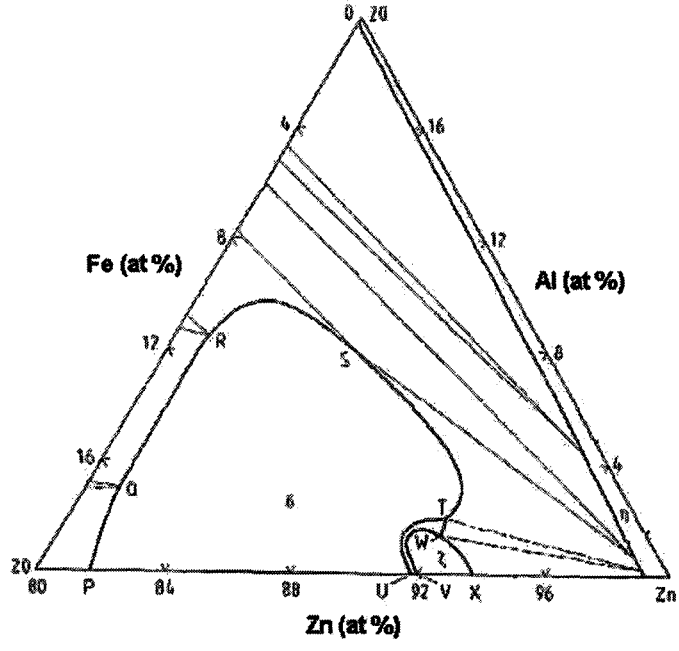

(b)

Figure 2-6: Evolution of Fe-Zn-Al phase diagram with time at 450°C, (a) equilibrium: >1000h (b) metastable: <30min. [Perrot *et al.*, 1992]

2.1.4 Determination of Dissolved Al in the Galvanizing Bath

As mentioned previously, both Fe and Al have a limited solubility in liquid Zn. The amount of Al dissolved in liquid Zn is commonly referred to in the industry as the "effective" Al. This term is used to distinguish between the dissolved Al and Al tied up in bath intermetallic particles. Due to the fact that the dissolved Al is the only Al available to react and form the inhibition layer, it is a significant parameter in the formation of the desired coating microstructure and properties for continuously galvanized products and determining a correct bath effective Al is quite important. This task has proven difficult due to the complex nature of the Zn-rich corner of the Zn-Al-Fe phase diagram [McDermid *et al.*, 2004 (B)], and many researcher have attempted to define the Zn rich corner of the Zn-Fe-Al ternary phase diagram [Belisle *et al.*, 1991] [Biele, 1995] [Perrot *et al.*, 1992] [Tang, 1998 (B)] [Tang *et al.*, 1995 (B)]. Although the phase relationships in the Zn corner of this system are extremely complicated and there are not extensive experimental data published on this subject, the Fe/Al solubility limit in the Zn-Fe-Al ternary phase diagram in the range used in continuous galvanizing and galvannealing bath compositions has been reported [Chen *et al.*, 1990 (B)] [Kaye *et al.*, 2005] [McDermid *et al.*, 2002 (B)] [McDermid *et al.*, 2004 (A)] [Tang, 2000] [Tang, 1996]. Figure 2-7 shows the phase diagram of the Zn-rich corner of the Zn-Al-Fe system at 470°C developed by Kaye, McDermid and Thompson [Kaye *et al.*, 2005].

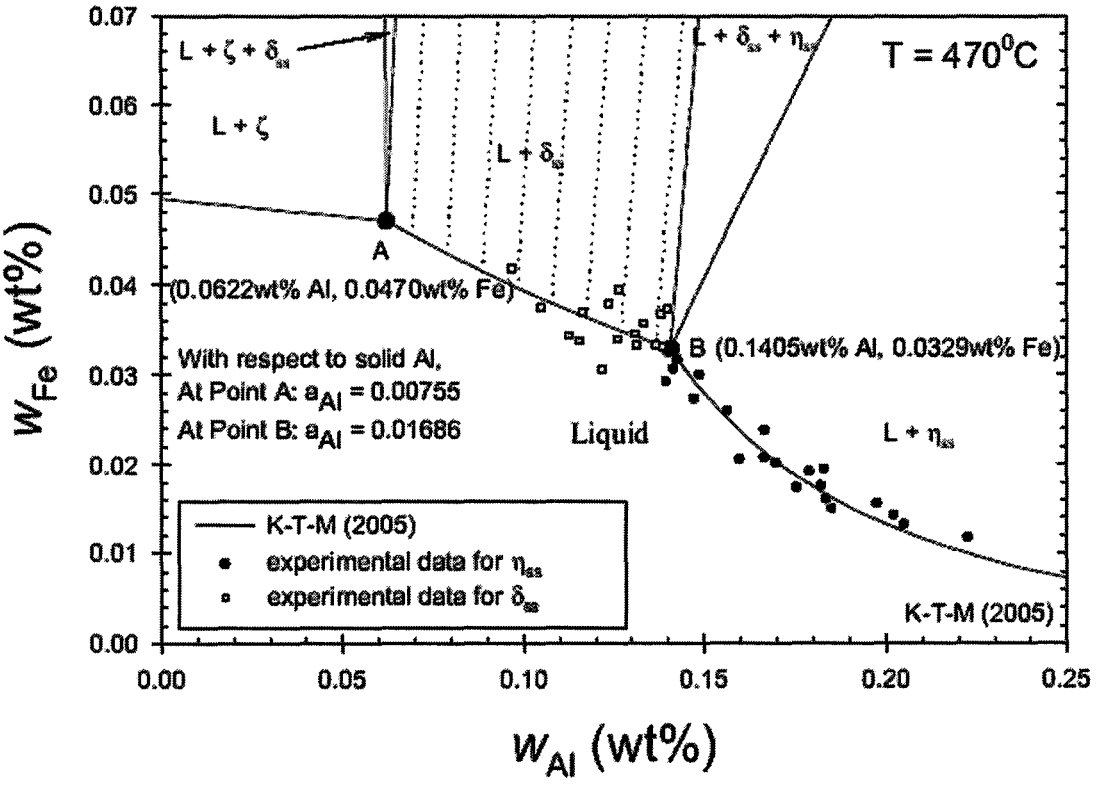

Figure 2-7: Phase diagram of the Zn-rich corner of the Zn-Al-Fe system at 470°C. [Kaye *et al.*, 2005]

2.2 Parameters Influencing Inhibition Layer Formation in Hot Dip Galvanized Coatings

There are several parameters identified as having a significant influence on the aluminum uptake at the interface (i.e. Al content of the Fe-Al interfacial layer), the formation of the Al-Fe inhibition layer and inhibition layer breakdown resulting in Fe-Zn intermetallic compound outbursts [Belisle, 1993]. These will be discussed in the following text.

2.2.1 Immersion Time

It was found that increasing reaction time between the steel substrate and zinc bath generally results in increased Al uptake and a greater thickness of the inhibition layer. Dubois [Dubois, 1998] showed the lower the line speed, and, therefore, the longer the immersion time, the higher the Al uptake when holding the remaining process variables constant. In Figure 2-8, Isobe [Isobe, 1992] showed that in the time required for steel to pass through the bath on a continuous galvanizing line, the majority of the total Al uptake in the coating occurs. In the first second of the immersion, high Al uptake was obtained and with the increasing immersion time, the Al content in the interfacial layer increases at a lower rate. This figure also shows that the Al content of the zinc bath has influence on the Al uptake. It should be noted that Isobe used "immersion time" to characterize the kinetics of the inhibition layer formation in his study. It should be emphasized that the immersion time is not the reaction time and it is simply the time the substrate is immersed in the bath. This is because it is likely that reactions, such as diffusional growth of the Fe-Al layer, continue to proceed until the coating has been solidified at approximately 420°C. Such post-immersion diffusion of Al after withdrawal of the steel sheet from the zinc bath and before solidification of the coating was discussed by some authors [Dubois *et al.*, 1993] [Faderl *et al.*, 1995] [Baril *et al.*, 1998] [Dubois, 2004]. Figure 2-9 shows the aluminum content of the bulk zinc coating – excluding the Fe-Al interfacial layer - varies with different cooling rates in a bath containing 0.25 wt% Al. It can be seen that the Al content of the zinc coating for samples with fast cooling is higher than those with slow cooling, and that the Al concentration in the bulk zinc coating is lower in comparison to

the bulk bath composition. Baril *et al* [Baril *et al.*, 1998] calculated the Al content in the interfacial layer by using the total Al content in the coating, in the bath and weight of the overlay ($w_{Al-coating} = w_{Al-ternary} + C_{Al-bath} \times w_{overlay}$). It was found that the calculated Al content in the interfacial layer is always less than the measured values when the bath contains 0.18 wt% Al and 0.16 wt% Al. It means that Al in the overlay diffuses to the interfacial layer to react with Fe and that growth of the interfacial layer continues during cooling and solidification of the coating.

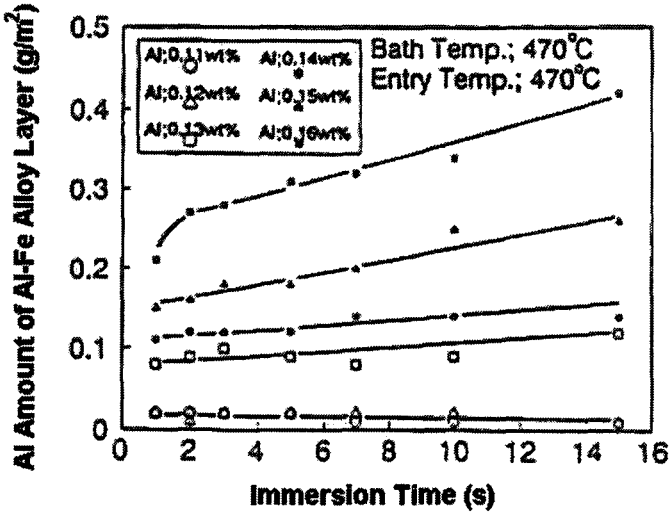

Figure 2-8: Al uptake of the Al-Fe alloy layer at 470°C for various bath Al contents and different immersion time [Isobe, 1992]

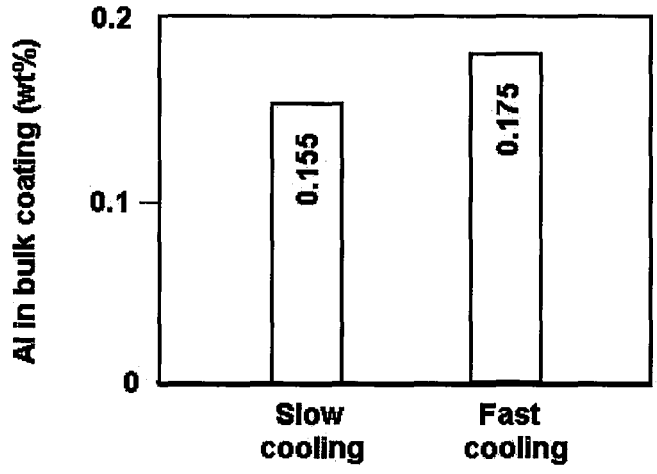

Figure 2-9: Aluminum content of the bulk zinc coating for slow cooling and for fast cooling (short time between withdrawal and solidification) [Faderl *et al.*, 1995]

2.2.2 Al content of the Zinc Bath

The Al content in the zinc bath has a great influence on the microstructure, morphology and Al uptake of the interfacial layer.

Morphology: the morphology of the Al-rich layer is strongly related to the Al content in the galvanizing bath [Baril et al., 1999]. According to the ternary Fe-Zn-Al phase diagram, when the dissolved Al content in the bath is below 0.14 wt% and above 0.10wt%, a partial inhibition layer is formed [McDermid *et al.*, 2002 (A)] [Inagaki et al., 1995] [Kiusalaas et al., 1989]. As shown in Figure 2-10, for lower dissolved Al contents of bath, the microstructure of the Al-rich layer has only one discontinuous sublayer with similar orientations, which shows colonies of grains with similar orientation. Tang [Tang, 1998 (A)] summarized the relationship between the coating microstructure in continuous galvanizing and the Al content of the bath, as show in Table 2-2. Here we should note

that, although δ phase is the equilibrium compound according to the Zn-rich corner of the Zn-Al-Fe phase diagram when the Al content of the bath is between 0.10-0.135 wt%, the formation of ζ phase is thermodynamically possible and kinetically favoured as the driving forces for the formation of these two phases, δ and ζ, are similar, but the ζ phase can grow epitaxially on the Fe substrate and the δ phase cannot. In this case, the Fe-Al layer has a fine granular structure, the ζ phase is pillar-like and δ phase is columnar [Marder, 2000].

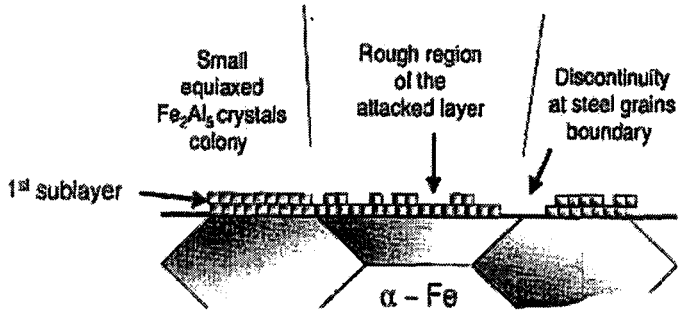

(a)

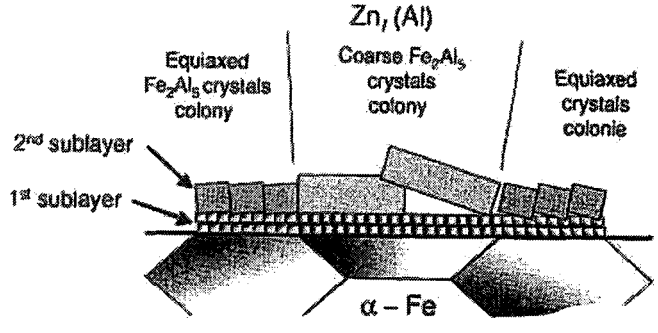

(b)

Figure 2-10: Schematic of the morphologies of the Al-rich interfacial layer formed in coatings obtained in bath with (a) 0.13 wt% and (b) 0.18 wt% dissolved Al [Baril *et al.*, 1999]

Table 2-2: Summary of coating microstructure in continuous galvanizing [Tang, 1998 (A)]

Al Content (wt%)	Equilibrium Compound	Intermetallics in Coating	Alloy Layer Characteristics	Nucleation Rate (s)	Growth Rate (μm/s)
<0.100	ζ ($FeZn_{13}$)	ζ/ δ/Γ'/Γ	Continuous	ζ~10^{18}	up to~10
0.100-0.135	δ ($FeZn_{10}$)	ζ/ δ/Γ'/Γ	Gaps exist	ζ~10^{18}	~1
0.135-0.140	η ($Fe_2Al_5Zn_x$)	ζ	Discontinuous	ζ~10^{15}	ζ~0.5, η~0.05
0.140-0.145		ζ , η	ζ dissolution	ζ η~10^{12}	ζ~0.1, η~0.05
0.145-0.150		η	ζ dissolution	η~10^{12}	η~0.05
>0.150		η	Full inhibition	η~10^{12}	η~0.05

When the Al content in the bath is above 0.14wt%, it is generally accepted that a full inhibition layer is formed. According to the study of Baril *et al* [Baril *et al.*, 1999], the microstructure of the Al-rich layer consists of two sublayers for high bath Al contents. The lower layer is composed of small compact equiaxed crystal and the upper layer, in contact with the Zn melt, has two morphologies. The first consists of small equiaxed crystals, and, the second, as shown in Figure 2-10, consists of coarse elongated crystals with a preferred growth orientation parallel to the substrate surface. Guttmann *et al*'s [Guttmann *et al.*, 1995] results also show that the lower interfacial layer with fine Fe-Al crystals has a preferred crystallographic orientation and the upper layer with coarse crystals exhibits apparently random crystalline orientation and morphologies.

Al uptake: Interfacial Al up-take increases with increasing dissolved Al content in the zinc bath, as shown in Figure 2-8. The results given by Toussaint *et al* [Toussaint *et al.*, 1998 (B)] also show that interfacial Al up-take increases with increasing dissolved Al content in the zinc bath between 0.14 wt% to 0.2 wt% and higher bath Al contents lead to high initial Al uptake. However, when the bath dissolved Al was greater than 0.2 wt%, a small reduction of interfacial Al up take was observed. The possible reason for this given was "more efficient mass transfer of Al in the melt towards the interface resulting in a complete coverage of the substrate with less matter". The stability of the inhibition layer was found to depend on the dissolved Al content in the baths. The inhibition layer obtained in the bath with the higher Al content was found to be more stable than that obtained in the bath with lower Al content. Results are illustrated in Figure 2-11.

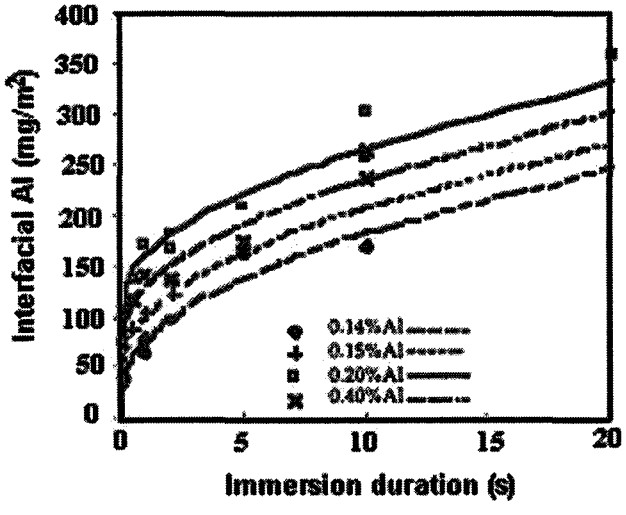

Figure 2-11: Effects of Al content on inhibiting layer formation. Melt and dipping temperature equal (460°C), turbulent condition. [Toussaint *et al.*, 1998 (B)]

A similar phenomenon was observed by Baril *et al* [Baril *et al.*, 1998]. The results, as shown in Figure 2-12, indicated that the total Al content in the coating increased with increasing Al content in the bath. Also, a significant value difference in Al content in the coating was obtained between bath Al contents below and above 0.15wt%. In high Al baths, high Al in the coating was observed and Al uptake was low, nearly constant, for low Al baths. In addition, the Al content of the interfacial layer was related to the reactivity of the steel, which depends on the solute additions in the steel. Combined with SEM observation, Baril *et al* [Baril *et al.*, 1998] pointed out that in the low Al bath (below 0.15wt%) the Fe-Al interfacial layer did not continue to grow during cooling and the Fe-Al interfacial layer growth was compensated by the formation of Fe-Zn intermetallic compound which consume it, as the Al content in the coating still continued to increase.

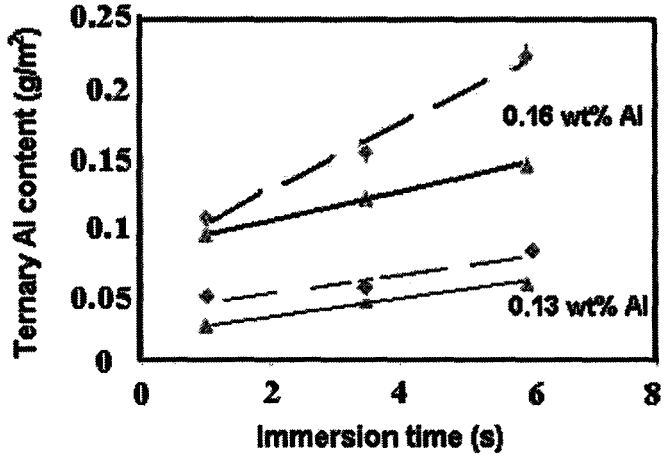

Figure 2-12: Al Content in the interfacial layer with two Al bath (3.5s immersion time, ♦ IF-Ti/Nb▲ULC) [Baril *et al.*, 1998]

2.2.3 Zinc Bath Temperature

The zinc bath temperature is another important parameter in the continuous galvanizing process and it has a significant impact on the Al uptake, morphology and grain size of the interfacial layer.

Aluminum uptake is expected to increase with increasing bath temperature and strip-entry temperature, because both work to increase the effective temperature of a strip for the formation and growth of Fe_2Al_5 at the interface i.e. it is the direct effect of temperature on growth kinetics [Tang, 1995 (A)].

The influence of bath temperature on the interfacial Al uptake was studied by Toussaint *et al* [Toussaint *et al.*, 1998 (B)]. The results, as shown in Figure 2-13, indicate that the Al content in the interfacial layer increases with increasing bath temperature. In addition, higher system temperature increased the initial Al up take and "seems to slightly accelerate growth kinetics". AFM (Atomic Force Microscope) images were also given as an additional proof of the influence of the temperature on system reactivity. Results revealed that interfacial layer roughness and mean grain size increased with temperature.

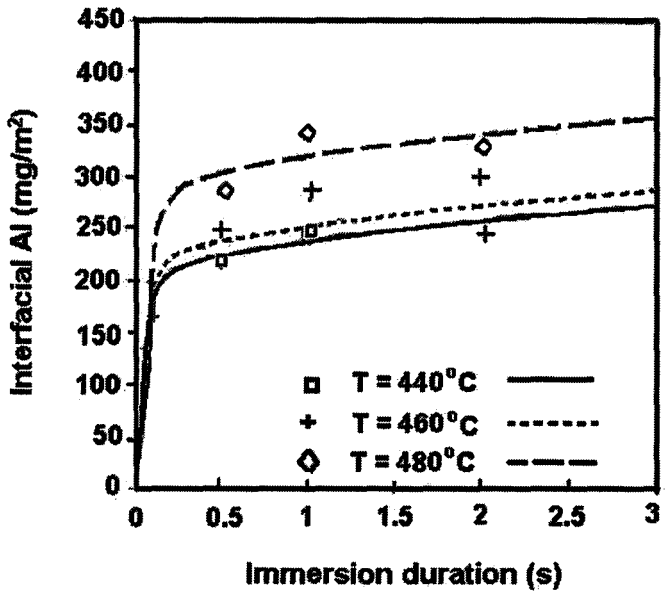

Figure 2-13: Effects of dipping temperature on inhibition layer formation. Melt and dip temperature equal, 0.2 wt% Al, laminar flow condition [Toussaint *et al.*, 1998 (B)]

However, the incubation period, which is the time for Fe-Zn outbursts to form and the inhibition layer to breakdown, decreases with increasing bath temperature [Yamaguchi *et al.*, 1979] [Proskurkin *et al.*, 1975], as shown in Figure 2-14. Because of the high diffusion rate of Zn and Fe at high dipping temperatures, it is easier for the Zn in the overlay to diffuse through the inhibition layer to form Zn-Fe intermetallic compounds at the grain boundary of the steel substrate. Thus, the Fe-Al interfacial layer becomes less stable with increasing temperature.

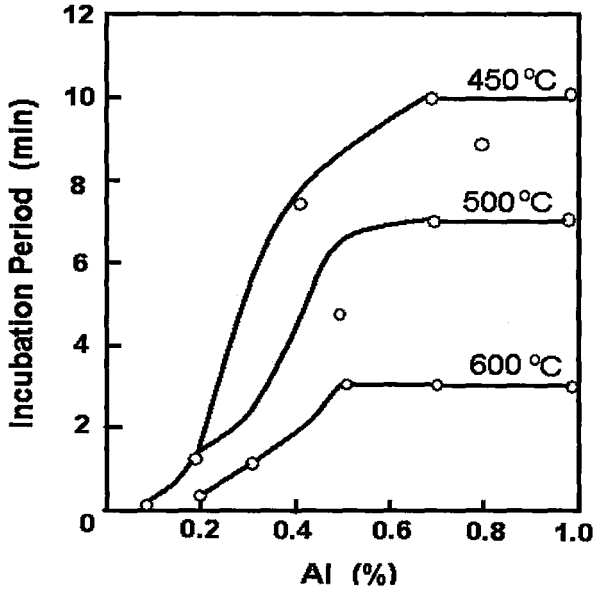

Figure 2-14: The dependence of the incubation period on the aluminum content and temperature of the molten zinc [Proskurkin *et al.*, 1975]

2.3 Phase Identification of the Inhibition Layer

Despite the industrial importance of galvanizing, there is a lack of detailed information about the composition, thickness and formation mechanism of the inhibition layer. This is because the Fe-Al layer that forms in commercial coatings are often too thin to be observed in cross-section using optical microscopy or conventional SEM. Similarly, the use of X-ray diffraction to identify the phase constitution and orientation of this layer is hampered due to the thickness of this interfacial layer [McDevitt *et al.*, 1997]. Many galvanizing researchers performed experiments to study the structure and composition of the inhibition layer, as summarized in Table 2-3. They investigated the inhibition layer by using different analytical method, such as SEM, EDS, XRD and TEM, often yielding conflicting results. Most authors believe that the inhibition layer is composed of a Zn-

bearing Fe_2Al_5 phase [Harvey *et al.*, 1973] [Faderl *et al.*, 1992; Saito *et al.*, 1991] [Tang *et al.*, 1993] [Guttmann *et al.*, 1995] [Price *et al.*, 1999]. However, some researcher have identified two Fe-Al intermetallic phases, Fe_2Al_5 and $FeAl_3$, in the inhibition layer [Lin *et al.*, 1995 (B)] [McDevitt *et al.*, 1997] [Morimoto *et al.*, 1997].

Table 2-3: Phase identification of the inhibition layer by different authors

Author	Analysis Method	Experimental Parameters	Characterization of the Inhibition Layer
Harvey [Harvey *et al.*, 1973]	XRD	0.18 wt% Al 450°C	$Fe_2Al_{(5-x)}Zn_x$ x is in the range 0.5 to 0.8
Faderl *et al* [Faderl *et al.*, 1992]	XRD EPMA		$Fe_2Al_{5-x}Zn_x$ x is equal to 0.5-0.8
Tang *et al* [Tang *et al.*, 1993]	EDS	0.144 wt% and 0.19 wt% Al 450°C	$Fe_2Al_5Zn_x$ x increased with increasing immersion time, from 0.6wt% for 3 seconds to 6.1wt% for 120 seconds
Guttmann *et al* [Guttmann *et al.*, 1995]	TEM	0.18 wt% Al bath 460°C	orthorhombic Fe_2Al_5 phase containing up to 23wt% Zn
Lin *et al* [Lin *et al.*, 1995 (A)]	TEM AEM	0.14 wt% Al	mixture of Γ_1, δ, ζ and $FeAl_3$ Zn-bearing Fe_2Al_5 and an Fe-Al-Zn ternary compound
McDevitt *et al* [McDevitt *et al.*, 1997]	TEM SEM XRD	0.20 wt% Al 470°C	layered structure of Fe_2Al_5 and $FeAl_3$
Morimoto *et al* [Morimoto *et al.*, 1997]	TEM SEM XRD	0.14 wt% Al	Fe_2Al_5 and $FeAl_3$ (the amount of these two phases are different on the Ti IF, Ti-Nb IF and P-added Ti IF substrate)
Hertveldt [Hertveldet *et al.*, 1998]	SEM and RBS	0.095-0.2 wt% Al 460°C -480°C	Fe-rich Fe-Al phase with 7 wt% Zn
	AES		compositional gradient Fe_2Al_5 or $FeAl_2/FeAl/Fe_3Al$
	TEM		$Fe_2Al_{5-x}Zn_x$ (2 wt %< x<20wt %)
Baril *et al* [Baril *et al.*, 1999]	XRD	0.10-0.20 wt% Al	isomorphous to Fe_2Al_5 crystal and the Fe/Al ratio close to that of Fe_2Al_5 22 wt% < Zn < 28wt%

2.4 Kinetic Models of Inhibition Layer Formation

It has been surmised that the formation of the inhibition layer is a three-stage process. The first stage comprises dissolution of Fe into the liquid zinc, due to the higher metastable Fe solubility in the vicinity of the strip/bath interface than the equilibrium Fe solubility in the balk bath; the second stage comprises nucleation of Fe-Al intermetallic compounds at the interface of the steel substrate and zinc bath, associated with a high rate of Al uptake; and finally, diffusion controlled growth [Tang, 1995 (A)].

Toussaint *et al* [Toussaint *et al.*, 1998 (C)] conducted experiments and built a mathematical model of inhibition layer formation in terms of the uptake of aluminum per unit area of interface as a function of time. The main conclusions were (1) nucleation was very fast and controlled by physico-chemical conditions, mainly temperature and aluminium supply from the melt (2) growth was slower when the layer was thicker, leading to the conclusion that growth was controlled by Fe diffusion through the existing layer and Al diffusion from the melt. Toussaint *et al* used the following equation, known as the Johnson-Mehl-Avrami model, to describe the two-stage formation kinetics of the inhibition layer:

$$Q = K\left(1 - e^{-Bt}\right) + At^{1/2} \tag{2.1}$$

The first term in the equation is representative of an almost instantaneous nucleation (approximately 0.1s according to their experimental results) associated with a high rate of Al uptake. The second term corresponds to solid state diffusional growth and a lower rate

of Al uptake. Diffusional growth will be dominant when the nucleation step is completed. K in the nucleation term is equivalent to an "initial" Al take-up, before diffusional phenomena takes control of the system. $K \cdot B$ is the slop of the initial Al take-up when diffusion is not taken into account. B is the "verticality" of initial growth, related to the nucleation time determined from the experimental results.

Toussaint *et al*'s calculations [Toussaint *et al.*, 1998 (C)] were based on the model developed earlier by Tang [Tang, 1995 (A)]. In Tang's model, the nucleus particle was assumed to be hemispherical in shape for mathematical simplicity. The free energy change associated with the formation of a hemispherical Fe_2Al_5 particle is expressed by:

$$\Delta G = \frac{\pi d^3}{12}\Delta G_v + \frac{\pi d^2}{4}\Delta\gamma \qquad (2.2)$$

Where d is the nucleus diameter, ΔG_v is the free energy change per unit volume associated with the formation of a hemispherical Fe_2Al_5 compound, $\Delta\gamma$ is the interfacial free energy change due to the formation of a hemispherical Fe_2Al_5 nucleus on the steel substrate in the zinc bath. ΔG_f, the free energy of formation of Fe_2Al_5, is given by:

$$\Delta G_f = -283{,}470 + 84.8 \cdot T(K) \quad \left[J \cdot mol^{-1}\right] \qquad (2.3)$$

Using the molar mass (M) of Fe_2Al_5 ($247\ g \cdot mol^{-1}$) and the density of Fe_2Al_5 ($4.125\ g \cdot cm^{-3}$), the free energy change associated with the formation of a hemispherical nucleus of Fe_2Al_5 per unit volume can be calculated as:

$$\Delta G_v = \frac{\Delta G_f}{M/\rho} = -4{,}734.1 + 1.4 \cdot T(K) \quad \left[J \cdot cm^{-3}\right] \tag{2.4}$$

The nucleation of Fe_2Al_5 on a steel substrate is a heterogeneous nucleation process. According to Tang's suggestion [Tang, 1995 (A)], the interfacial free energy change, $\Delta\gamma$, is equal to $1.21 J \cdot m^{-2}$ .The critical nucleus size (d^*) can be easily computed by differentiation of equation (2.2) with respect to d and setting the derivative equal to zero:

$$d^* = \frac{-2\Delta\gamma}{\Delta G_v} \tag{2.5}$$

Thus, the energy barrier for the formation of a critical nucleus, ΔG^*, can be calculated. According to the expression for the nucleation rate, the number of nuclei per unit surface (n) that have reached the critical size is given by:

$$n = \Omega \cdot \exp\left(-\frac{\Delta G^*}{kT}\right) \tag{2.6}$$

Where Ω is the number of nucleation sites of iron atoms per unit surface and equals to $1.92 \times 10^{19} m^{-2}$. k is the Boltzmann constant ($1.38 \times 10^{-23} m^2 \cdot kg \cdot s^{-2} \cdot K^{-1}$). The mass heterogeneous nucleation rate for the formation of a Fe_2Al_5 particle at the steel-bath interface is equal to $K \cdot B$ and is given by:

$$K \cdot B = 27000 \cdot \frac{f}{N_a} \cdot C_{Al} \cdot \Omega \cdot \exp\left(-\frac{\Delta G^*}{kT}\right) \quad \left[mg \cdot m^{-2} \cdot s^{-1}\right] \tag{2.7}$$

In this expression, f is a complex function that depends on the vibration frequency of the atoms, the activation energy for diffusion in the liquid and the surface area of the critical nuclei. It is sufficient to consider it a constant equal to $\sim 10^{11}$ [Porter *et al.*, 1992]. N_a is

the Avogadro number (6.02×10^{23}). C_{Al} is the initial surface fraction of Al atoms, which is calculated from its volume concentration value. Toussaint *et al* made some modifications to this term by applying two correction factors:

$$\Omega = 1.92\times10^{19}\cdot\frac{V_{unit}}{4V^*}\cdot\frac{\pi}{2} \qquad \left[m^{-2}\right] \tag{2.8}$$

Here, V^* is the critical nucleus volume and V_{unit} is the volume of the Fe_2Al_5 unit cell ($2.07489\times10^{-28}m^3$). When the nucleation term has reached 99% of its final value, B can be calculated by:

$$B = -\frac{1}{t_c}\ln 0.01 \qquad \left[s^{-1}\right] \tag{2.9}$$

In the above equation, t_c is the critical time and was estimated from experimental results. Thus, when the bath temperature and Al content in the bath are fixed, the initial Al take-up, K, can be easily obtained in $mg\cdot m^{-2}$.

The value of A in the diffusional growth term was estimated by the following equation:

$$A = f\cdot A_{boundaries} + (1-f)\cdot A_{crystal} \tag{2.10}$$

$$A^2 = \left(\frac{135^2}{112^2}\right)\cdot 2\cdot D\cdot \Delta C\cdot \rho\cdot \phi \tag{2.11}$$

Where f is a adjustable factor. Its value is close to 1 and may decrease slightly when the layer thickens. $(135/112)$ is the Al / Fe mass ratio in the Fe_2Al_5 molecule. D is a diffusion constant determined by using Rutherford backscattering results on Fe-Al diffusion couples and has different values for diffusion in the lattice and for diffusion in

grain boundaries [Teixeira *et al.*, 1987]. ΔC is the change in Fe concentration from one side of the inhibition layer to the other and its value was estimated to be approximately $50\times10^{6} mg\cdot m^{-3}$. ρ is the density of the inhibition layer, and ϕ is the mass fraction of iron in the inhibition layer and its value is equal to 112/247. Values used in this model are summarized in Table 2-4.

Table 2-4: Various values for mathematic model

Parameter	450°C	460°C	470°C	480°C
$\Delta G_V\left(J\cdot cm^{-3}\right)$	-3710	-3696	-3682	-3668
$d^*(m)$	6.52E-10	6.55E-10	6.57E-10	6.6E-10
$\Delta G^*\left(J\cdot mol^{-1}\right)$	1.35E-19	1.36E-19	1.37E-19	1.38E-19
$K\cdot B\left(mg\cdot m^{-2}\cdot s^{-1}\right)$	3774.77	4041.05	4331.57	4606.97
$A_{broundary}$	48.10	49.87	51.66	53.46

Setting the value of the critical time (t_c) to 0.1s to and setting the value of the diffusion factor (f) to 1, experimental results, obtained when the Al content of the bath was 0.2 wt%, the bath temperature was 460°C and the hydrodynamic condition was turbulent, were compared to the above model, as shown in Figure 2-15. Toussaint *et al* found that this model gave satisfactory agreement with their experimental results.

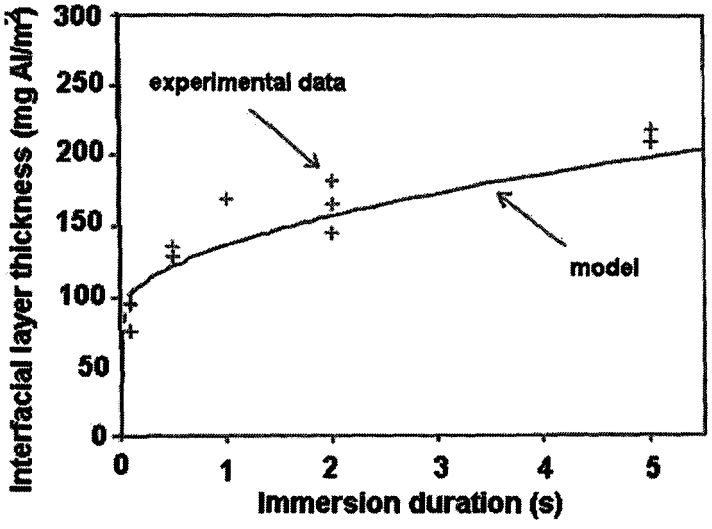

Figure 2-15: Prediction of the mathematical model with experimental results [Toussaint *et al.*, 1998 (C)]

Giorgi and Guillot [Giorgi *et al.*, 2004] developed a model for the kinetics of galvanizing reactions and quantified Fe and Al exchange between the steel and liquid zinc as a function of immersion time. In their model, growth of the interfacial layer was divided into three steps: the first step, nucleation, occurs at the interface and leads to the formation of spherical nuclei; in the second step, the crystals grow laterally until the steel surface was completely covered and the crystals are cubic in shape; in the third step, the crystals grow perpendicular to the steel surface. This model was based on solving the diffusion equations for iron and aluminum in the bath to obtain the concentration profiles of iron and aluminum as a function of immersion time and space perpendicular to the steel surface, given by:

$$D_{Fe}^{Zn(L)} \frac{\partial^2 c_{Fe}}{\partial z^2} = \frac{\partial c_{Fe}}{\partial t} \tag{2.12}$$

$$D_{Al}^{Zn(L)} \frac{\partial^2 c_{Al}}{\partial z^2} = \frac{\partial c_{Al}}{\partial t} \tag{2.13}$$

In the above two equations, $D_{Fe}^{Zn(L)}$ and $D_{Al}^{Zn(L)}$ are the diffusion coefficients of Fe and Al in the zinc bath ($m^2 \cdot s^{-1}$). c_{Fe} and c_{Al} represent the Fe and Al concentration in the bath ($mol \cdot m^{-3}$), and z is the space variable in the direction perpendicular to the steel surface (m).

They compared their calculation results for the mass of Al in the interfacial layer with the experimental results of Toussaint *et al* [Toussaint *et al.*, 1998 (A)] and pointed out that the growth of the interfacial layer starts after a delay of about 0.1 second, which is the time needed for iron to reach supersaturation. The growth rate is very high from 0.1 second to 0.4 second and then decreases significantly. The experimental results for 0.2 wt% Al containing Zn baths with saturated Fe and a 460°C bath temperature from Toussaint *et al* were fit well by this model, as shown in Figure 2-16. Thus, they believe that the interfacial Al measurements at 0.1 second were probably overestimated because of the cooling time during which growth continued. As an example, their model was used to assess prospective short time contact results. The calculations showed that all reactions were completed within approximately 0.5 second. Figure 2-17 shows their modeling results concerning the iron mass balance as a function of immersion time. We can see that both reactions were completed within 0.5 second. However, this short contact time model was not validated by any laboratory experiments.

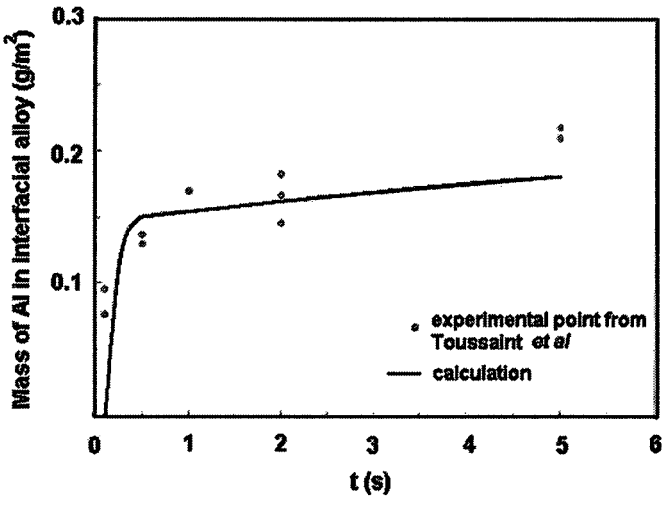

Figure 2-16: The model of Giorgi *et al* vs. the experimental points from Toussaint *et al* [Giorgi *et al.*, 2004] [Toussaint *et al.*, 1998 (A)]

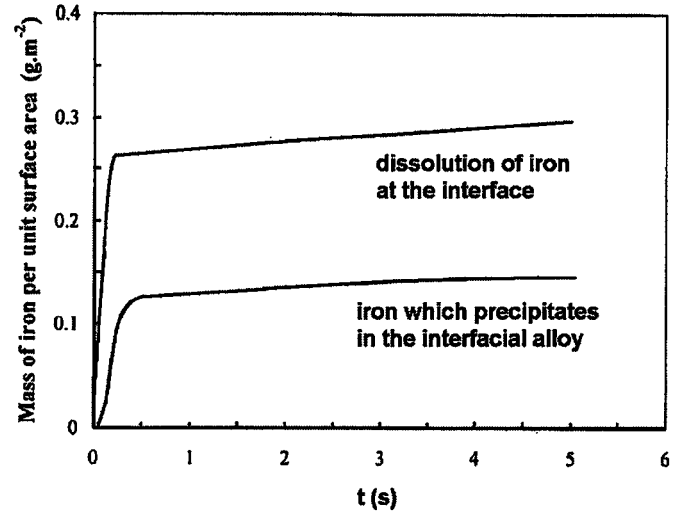

Figure 2-17: Iron mass balance as a function of immersion time [Giorgi *et al.*, 2004]

Guttmann [Guttmann *et al.*, 1995] also explained the two-stage growth kinetics of the interfacial layer by observations of the microstructure and composition of this layer. The

very short time (less than 1 second) initial growth period would correspond to the formation of the lower small crystal layer until these crystals meet each other and form a compact layer. This initial stage corresponds to a very rapid interface-controlled reaction (probably with linear kinetics), as the substrate remains in contact with the liquid. The formation of the upper, coarse crystal, layer would correspond to the slower stage that is control by the solid state diffusion of Fe through the already formed fine crystal layer.

2.5 Previous Studies on Short Time Inhibition Layer Formation

As mentioned in the section of kinetics of inhibition layer formation, we surmise that nucleation and diffusional controlled growth are the two steps of inhibition layer formation. Moreover, it is believed that the inhibition layer is nucleated at very short times (i.e. less than one second). However, short time inhibition layer formation has been studied only by a few authors because of the experimental difficulties.

Toussaint *et al* and Winand *et al* performed some experimental and modeling work on the nature of aluminum pick-up at short immersion times [Toussaint *et al.*, 1998 (A)] [Toussaint *et al.*, 1998 (B)] [Toussaint *et al.*, 1998 (C)] [Winand *et al.*, 1997]. A hot dip galvanizing simulator was used in these studies in an attempt to determine the reaction kinetics of the inhibition layer formation including nucleation kinetics. In their studies, they used a translational speed for the pneumatic actuator of 2 ms^{-1} and the shortest residence time of the top of the sample in the zinc bath was 0.1s. An example of their

experimental results is shown in Figure 2-18. In their experiments, the hydrodynamic conditions in an industrial galvanizing bath were simulated by making use of a vertical hollow cylindrical sample dipped in a zinc bath contained in a rotating crucible such that the Reynolds numbers were 2000, 3800 and 4500. Laminar conditions were also studied and were characterized by smooth, constant fluid motion.

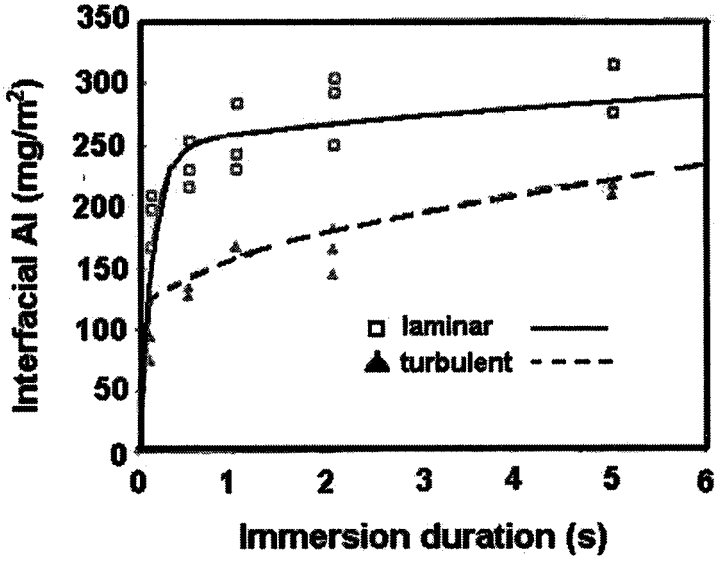

Figure 2-18: Experimental results concerning the interfacial Al pick-up (0.2 wt% Al; melt and dip temperatures equal to 460°C; laminar and turbulent conditions) [Toussaint *et al.*, 1998 (A)]

Two domains that were not explored previously, short immersion times of greater than or equal to 0.1 second and hydrodynamic condition, were investigated to determine their effect on the formation of the inhibition layer. From the experimental results, some conclusions were drawn concerning the effect of bath composition, immersion temperature and hydrodynamics on Al take up at the interfacial layer. Their results

showed that "the aluminum pick-up was very rapid, most of the layer being built in a few tenths of a second and subsequent thickening is slightly slower" [Toussaint *et al.*, 1998 (B)]. It was also shown than interfacial Al uptake increased with increasing dissolved Al in the zinc bath, immersion time and bath temperature. Turbulent conditions resulted in a significant decrease of the Al uptake without impairing the inhibition quality.

However, there are a couple of issues in the above studies which should be carefully considered. First of all, the shortest immersion duration for their study was 0.1 second. They were not able to determine the value of the interfacial Al content for immersion durations of less than 0.1 second. Thus, the point of interfacial Al up-take at 0.1 second should have been the first experimental point on the above figure. When the authors created the trendline for all experimental data, they shouldn't have extended the trend line to the range where the immersion duration was less than 0.1 second.

Secondly, we surmise that there are three reaction steps occurring after the steel sheet enter the zinc bath. Initially, Fe is dissolved from the steel strip surface by the bath due to higher metastable Fe solubility in the vicinity of the strip/bath interface. After the dissolved Fe solubility reaches a supersaturated level with respect to the equilibrium solubility of Fe, stable Fe-Al intermetallic clusters are established, i.e. nucleation of the inhibition layer, followed by diffusional growth. This means there may be an incubation period before the inhibition layer nuclei formation, although we currently don't know

how long this time is. Thus, during this period, no interfacial Al pick up can be measured. Thus, the trendline in Figure 2-18 should not be connected to the point "0".

Third, the authors mentioned in their work that the shortest immersion time of the top of the sample in the zinc bath was 0.1s. Based on the experiments, they concluded that the aluminum pick-up was very rapid and that most of the layer was built in a few tenths of a second. Here, there was confusion between immersion time and reaction time. In their experiments, after immersion in the zinc bath for a given time, the sample was then quickly moved to the sample introduction chamber where it was cooled using a high flow nitrogen quench which solidified the zinc coating in approximately 10 seconds (start of solidification after 6 seconds and 100 – 150°C after 20 seconds) [Toussaint *et al.*, 1998 (A)]. The problem is that the nucleation and growth reactions did not likely stop during the unknown time between withdrawal of the sample and solidification of the coating which means that the reaction time between the bath and Fe was actually likely much longer than the immersion time of 0.1s . Thus, the model outlined in the previous section likely contains some significant errors in the values of the parameters due to an incorrect estimate of the critical reaction time t_c [Toussaint *et al.*, 1998 (C)]. Furthermore, the data presented in Figure 2-18 likely needs to be shifted to longer times if one is to utilize reaction time for the kinetic model.

2.6 Objectives of the Present Study

Based on the discussion concerning the short time formation of the galvanizing inhibition layer, the reaction time is a crucial parameter to consider when investigating the formation of the inhibition layer. Thus, the objectives of the present study were established as follows:

(1) Develop a better understanding of the formation of the inhibition layer at short *reaction times*. It is believed that the inhibition layer is formed in a very short time. A literature survey showed that the mechanism of short time inhibition layer formation was studied only by a few people because of experimental difficulties. Even so, they used dipping time or immersion time to characterize the inhibition layer formed at short times and ignored the cooling time to solidify the coating and arrest the reaction between the zinc bath and steel substrate. An objection of this project is to investigate inhibition layer formation as function of actual reaction time.

(2) A novel approach (galvanizing simulator and helium spot quench for *rapid cooling*) will be used to determine the effects of reaction time, bath chemical composition and bath temperature on the morphology and Al uptake of the inhibition layer. Both galvanizing and galvannealing bath composition will be used. The immersion time will focused on short times, mainly less than 1 second. The range of reaction temperature will be from 460°C to 480°C.

(3) Develop a modified model to describe the kinetics of inhibition layer nucleation and growth as a function of reaction time.

CHAPTER 3. EXPERIMENTAL METHOD

3.1 Experimental Materials

Steel coupons used for this project were provided by Stelco Inc and consisted of Ti stabilized-IF steels. The chemical composition of the experimental steels is given in Table 3-1. The steels were provided in the form of 1 mm thick panels in the cold rolled condition.

Table 3-1: Chemical composition of Ti-IF steel

Element	C	Mn	P	S	Si	Ni	Nb	Ti	Al	N
wt%	0.003	0.14	0.006	0.007	0.007	0.015	0.017	0.050	0.032	0.002

3.2 Experimental Apparatus

3.2.1 Galvanizing Simulator

The McMaster Galvanizing Simulator (MGS, Iwatani-Surtec) (Figure 3-1) was used to simulate the annealing and hot dip coating processes. The simulator is capable of simulating processes such as annealing, cooling, hot dip coating (Zn, Al, etc.), galvanizing and galvannealing at the laboratory scale.

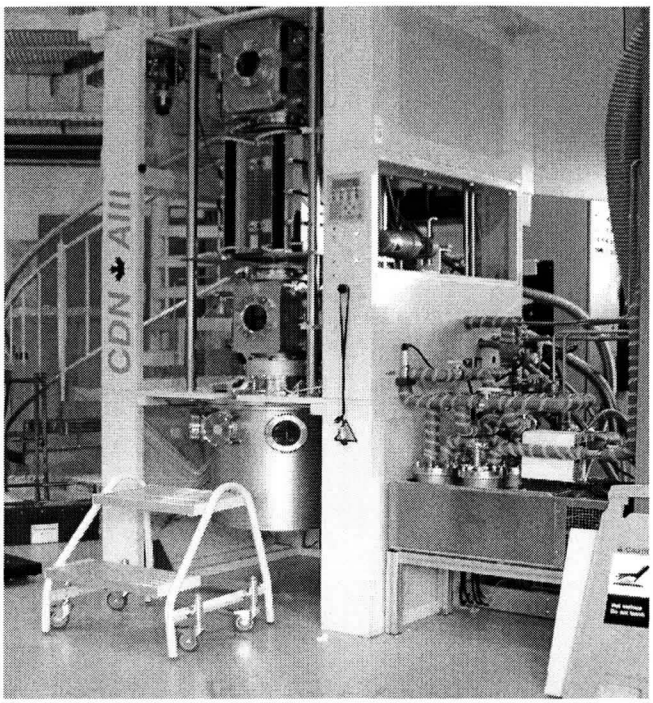

Figure 3-1: General view of McMaster galvanizing simulator

The simulator consists of three functional units: (1) the main unit, as shown in Figure 3-2, including drive mechanism, process chambers, infrared furnace, induction furnace, molten metal bath; (2) gas mixing stations; and (3) system control. The drive mechanism allows for rapid and precise movement of the sample to each process region of the MGS. The upper chamber is used for the loading and unloading of samples and contains two parallel cooling plates. The infrared furnace is used for most heat treatment cycles. The process gases, typically N_2, H_2, and He are premixed in the gas mixing station and then fed into the process chambers directly or through a humidification system to achieve the desired dew points to control the oxygen potential of the process gas. The induction furnace is used primary for galvannealing simulations and was not used in the present

work. The upper chamber (with sample & cooling chamber) and lower chamber (with molten metal bath, guide roll system and wipers) are separated by a pneumatically controlled gate valve. This valve allows evacuation of the upper chamber at the beginning of each test cycle. The lower chamber, with its relatively small gas volume, is kept oxygen free by continuous N_2 purging. The 50kg graphite crucible contains the molten zinc alloy for coating. The Zn pot is heated by a resistance furnace controlled by a type K thermocouple.

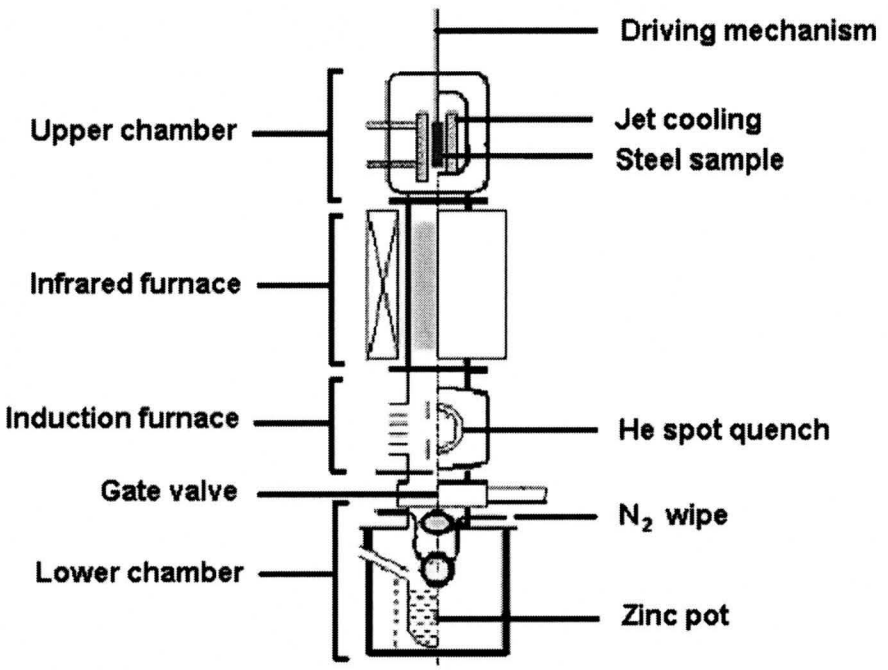

Figure 3-2: Schematic design of the McMaster galvanizing simulator

Steel samples are typically heated in the infrared furnace and then dipped into the molten zinc pot. After dipping, the steel samples are gas jet wiped to control the coating weight and usually cooled in the upper chamber by flowing nitrogen gas. There are two

problems that should be considered carefully. First, nitrogen jet cooling is not capable of cooling at sufficiently high rates to achieve the desired solidification times of the coating for the present work. Secondly, it takes several seconds for the sample to reach the upper chamber. In the present project, we wanted to solidify the zinc coating in a very short time to reduce and control the total reaction time. To achieve this, the helium spot cooler (Figure 3-2) was used to solidify the zinc coating as rapidly as possible immediately following nitrogen wiping in order to arrest the reaction between the substrate and molten zinc. In this design, it required less than 2 seconds for the sample to reach the helium spot cooling position after leaving the zinc bath. During spot cooling, the helium flow rate was set to 500 L/min and a helium flow time of 4s was used. Under this condition, the cooling rate for the coating reached approximately 100°C/s.

3.2.2 Experimental Procedure

Steel samples are first washed in a 2-3wt% sodium hydroxide solution using nylon brushes to remove dirt and other organic contaminants and then rinsed with distilled water. Coupons were further cleaned in the ultrasonic cleaner with isoproponal and dried using warm forced air. Immediately before putting samples into the MGS, a final cleaning was performed by wiping with acetone.

Steel samples used for this project consisted of 200mm×120mm×1mm coupons, with the 200mm axis parallel to the rolling direction. Two K type thermocouples were welded onto the steel sample surface. The first thermocouple was placed above the galvanizing

line and was used to control the sample thermal cycle. The second thermocouple was placed on the quench cooling spot to measure the temperature during the spot quenching. Figure 3-3 shows the steel sample dimensions, the two thermocouple wires and the spot quench position.

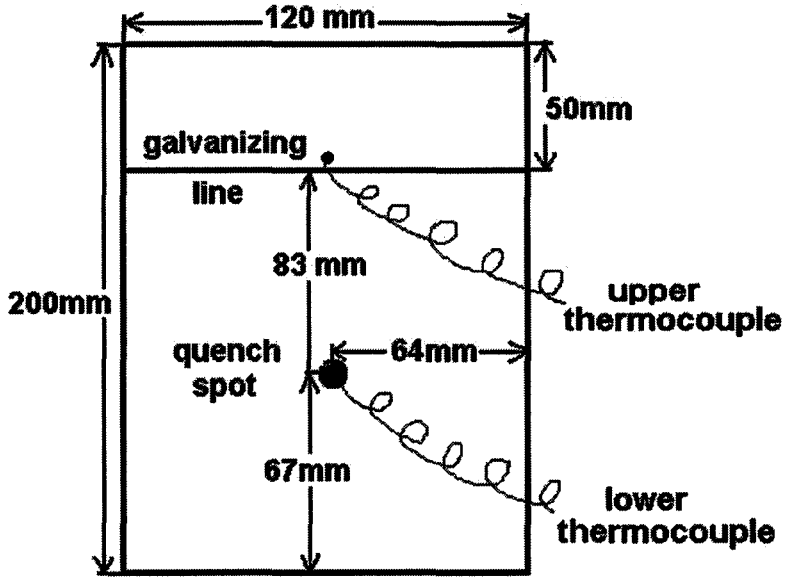

Figure 3-3: Schematic figure of dimension for steel sample

For the simulation experiments, the sample was placed onto the drive rod through a door in the upper chamber. Reduction gas (95% N_2, 5% H_2) was introduced into the column following several vacuum purges and backfills. The flow rates of nitrogen and hydrogen were set to 40 and 2.1 L/min, respectively. The reduction gas dewpoint was set to -30°C (i.e. $P(H_2O)/P(H_2) = 0.008$). The sample then entered the infrared annealing furnace for recrystallization and surface oxide reduction annealing. The target temperature was

750°C and the sample was held for 120 seconds in the annealing furnace. A typical annealing cycle is shown in Figure 3-4. The sample was then moved into the upper chamber, where it was cooled to 570°C at a rate of 20°C/s, and returned to the induction furnace, where it was cooled to the dipping temperature (460°C) by nitrogen gas at 2°C/s. The flow rate of nitrogen gas was set to be 400L/min during the cooling stage. The steel sample then passed through the gate valve which separates the upper section from the molten zinc pot at 500 millimeters per second, was dipped in the molten zinc bath for the target immersion time, then left the bath with the unsolidified zinc coating at 500mm/s through the gas jet wiper and reached the fast cooling position, where helium gas was applied for rapid cooling. The flow rate of helium was set to be 500 L/min to ensure a high cooling rate (over 100°C/s) to effectively arrest the reactions between the zinc coating and the steel substrate in a very short time. The coated sample then moved to the upper chamber, where the sample was cooled by nitrogen gas with a flow rate of 500 L/min to room temperature from both sides, after which the sample was removed.

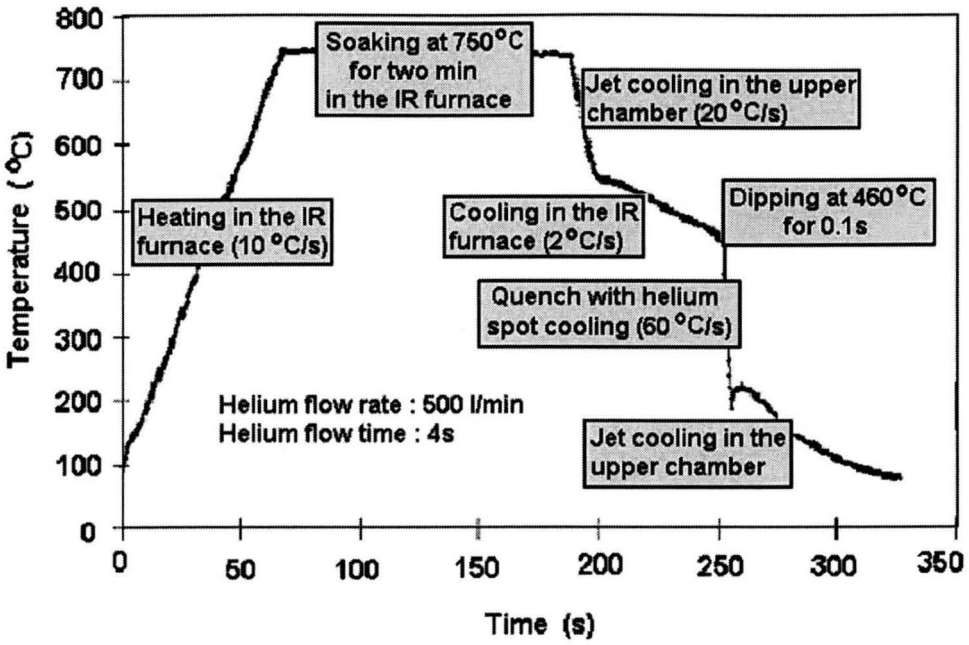

Figure 3-4: Typical annealing cycle for steel samples

3.2.3 Reaction Time Calculation

It was mentioned previously that the dipping time is not equivalent to the reaction time and the present work is based on the latter time. Thus, the calculation of the total reaction time is crucial. The following section summarizes the technique used to calculate the reaction time, using the thermal profile of sample USC07 as an example.

Figure 3-5 shows the temperature and position profile of sample USC07. In this figure, the blue curve and pink curve show the temperatures for the upper thermocouple and spot cooling thermocouple, respectively, during the experiment. The green curve indicates the

position of the steel sample in the simulator; this data is based on the distance between the bottom of the steel sample and the reference position- i.e. ground.

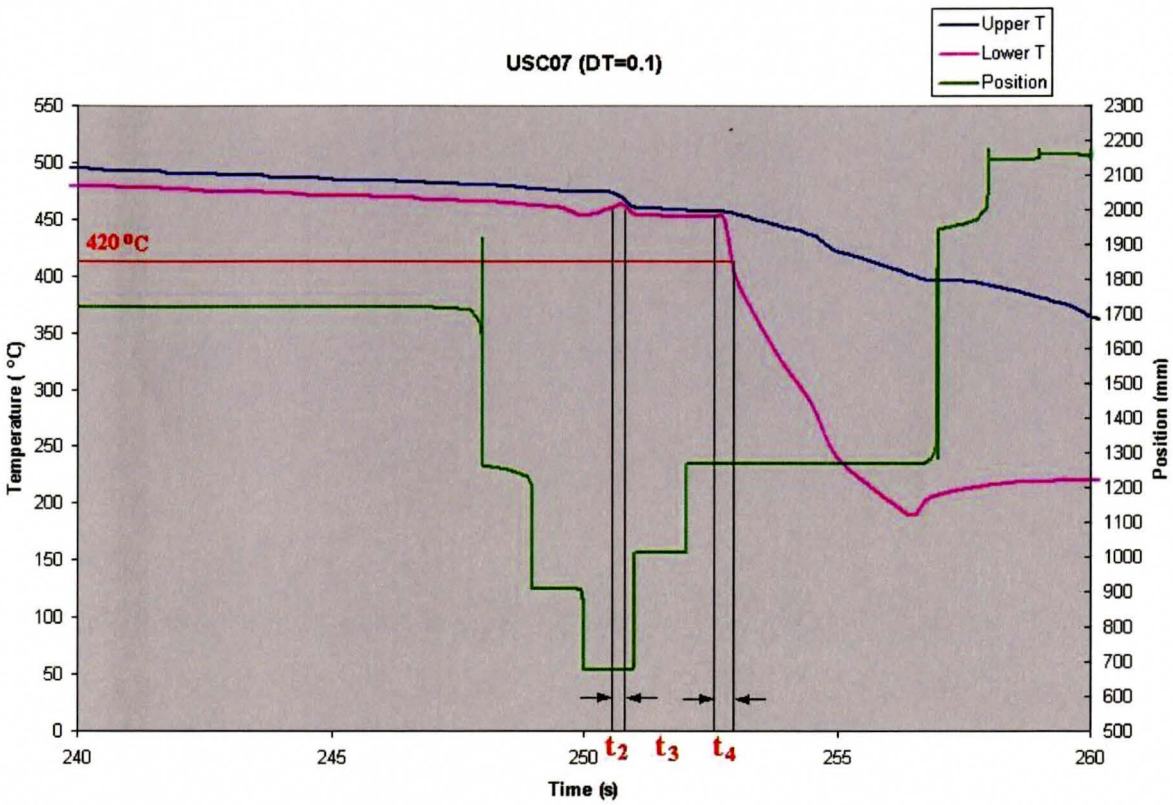

Figure 3-5: Temperature and position profile for sample USC07

Calculating the total reaction time is based on the sum of four times, t_1, t_2, t_3 and t_4, as shown in Figure 3-5.

Before the dipping time is measured, the spot cooling position on the steel sample has already contacted the zinc bath. Thus, t_1 is the difference between the time when the rapid cooling spot contacts with zinc bath and the time when the dipping time was started,

which can be calculated using the distance between the quench spot and the galvanizing line (Figure 3-3) and the sample dipping speed such that:

$$t_1 = \frac{83mm}{500mm/s} = 0.166s \tag{3.1}$$

Here, t_2 is the dipping time and, for this sample, $t_2 = 0.1$ s can be obtained directly from Figure 3-5.

t_3 is the difference between the time at which the sample left the zinc bath and the time at which the sample reached the spot cooling position. In this example, we know that the sample left the zinc bath at 255.875 s and reached the spot cooling position at 252.5 s from the position vs. time data. Thus,

$$t_3 = 252.5 - 250.875 = 1.625s \tag{3.2}$$

t_4 is the time taken to arrest the liquid metal-substrate reactions after helium spot cooling starts and is the time difference between the sample reaching the spot cooling position and the temperature at the spot cooling position dropping below 420°C, i.e. the solidification point of pure Zn. Thus, it is assumed the reaction rate decreases significantly when the temperature is below 420°C, i.e. liquid reactions are much faster than solid state reactions. According to the spot cooling thermocouple profile, we know that the temperature was 451.9°C at 252.5s and the temperature decreased rapidly to 397.9°C at 253s. This gives an average cooling rate of 108°C /s. If we assume that the

cooling rate during this period was constant, t_4 can be calculated by the following equation:

$$\frac{1s}{108^{o}C} = \frac{t_4}{31.9^{o}C} \tag{3.3}$$

Here, 31.9°C is the temperature difference between 451.9°C and coating solidification temperature (420°C). Therefore, t_4 = 0.295s, i. e., it takes 0.295 s for the zinc coating to solidify after reaching the spot cooling position.

The total reaction time is the sum of t_1 through t_4, given by:

$$t_{totoal} = t_1 + t_2 + t_3 + t_4 = 2.186 \text{ s} \tag{3.4}$$

For other samples with different dipping times and molten zinc bath temperatures, the total reaction times were different. However, because the dipping speeds were the same (i.e. 500mm/s) for all the samples, t_1 and t_3 have the same value for all samples. For t_4, it should be mentioned that when the steel sample left the molten zinc bath, it had the same temperature as the zinc bath and there was approximately a 10°C decrease of the zinc coating overlay temperature when the steel sample reached the helium spot cooling position according to the temperature and position profile. This means that a longer cooling time (t_4) was needed for samples which were dipped into higher temperature baths. Actually there were some slight variations in t_4 between samples due to slightly different cooling rate. Table 3-2 summarized the reaction time for all samples used in this project. These typical reaction time calculations were based on the following assumptions:

(1) the cooling rate of the helium cooling spot zinc overlay was the same for all the samples and (2) the reaction between the zinc coating overlay and steel substrate was arrested when the temperature was below 420°C.

Table 3-2: Reaction time calculation

Sample/Bath Temperature	t_1 (s)	t_2 (s)	t_3 (s)	t_4 (s)	Total reaction time (s)
450°C	0.166	0.1s / 0.3s / 0.5s/ 1s / 3s / 5s	1.625	0.185	1.976+ t_2
460°C	0.166	0.1s / 0.3s / 0.5s/ 1s / 3s / 5s	1.625	0.295	2.086+ t_2
470°C	0.166	0.1s / 0.3s / 0.5s/ 1s / 3s / 5s	1.625	0.37	2.161+ t_2
480°C	0.166	0.1s / 0.3s / 0.5s/ 1s / 3s / 5s	1.625	0.463	2.254+ t_2

3. 3 Experimental Parameters

Many parameters [Belisle, 1993] [Hertveldet et al., 1998] were identified which can influence the reaction between the zinc coating and steel substrate. For the present experiments, the following parameters were chosen to study the interfacial reaction: immersion time, bath composition and bath temperature. Table 3-3 summarizes the experimental matrix. All Zn baths used in the experiments were supersaturated with respect to Al and Fe. The bath composition was analyzed by ICP and the dissolved Al

and Fe contents calculated via the phase diagram of McDermid *et al* [McDermid *et al.*, 2004 (B)].

Table 3-3: Experimental parameters

Bath Temperature (°C)	Bath Composition				Immersion Time
	Total Al (wt %)	Total Fe (wt %)	Dissolved Al (wt %)	Dissolved Fe (wt %)	
450°C	0.144	0.033	0.1326	0.0214	0.1s / 0.5s/ 2s / 5s
460°C	0.144	0.033	0.1366	0.0265	0.1s / 0.5s/ 2s / 5s
460°C	0.133	0.032	0.1324	0.0268	1s / 2s
470°C	0.144	0.033	0.1424	0.0317	0.1s / 0.5s/ 2s / 5s
450°C	0.218	0.021	0.2037	0.0098	0.1s / 0.3s / 0.5s/ 1s / 3s / 5s
460°C	0.218	0.021	0.211	0.0156	0.1s / 0.3s / 0.5s/ 1s / 3s / 5s
470°C	0.214	0.019	0.2058	0.0126	0.1s / 0.3s / 0.5s/ 1s / 3s / 5s
480°C	0.214	0.019	0.2099	0.0158	0.1s / 0.3s / 0.5s/ 1s / 3s / 5s

3. 4 Analytical Procedure

3.4.1 Determination of coating Al (ICP)

The fast cooling spot was first cut from the steel panel. The area of the quench spot was determined by using an optical stereoscope coupled with an image analysis system (ZEISS Stemi 2000-C).

The coating overlay (i.e. metallic Zn layer) was stripped using the procedure "Zinc products and applications – galvanized coatings selective stripping procedure" provided by Noranda Inc. [Noranda]. This procedure consists of the following steps: 1) wipe the sample with acetone to degrease; 2) cover the opposite side with electrogalvanizer tape for testing only one side of the coupon; 3) pour fresh fuming nitric acid into a beaker; 4) immerse the coupon with polymer pliers (total reaction time is 6 to 12 seconds depending on coating weight); 5) remove sample when the surface is uniformly matte grey in appearance (i.e. the colour of the Fe_2Al_5 interfacial layer); 6) rinse the sample with acetone; 7) remove the protective tape and rinse the sample with acetone. After these steps, the zinc overlay and any Fe/Zn intermetallics in the galvanized coatings are dissolved and only the Al-rich interfacial layer remains.

To measure the Al-content of the Al-rich interfacial layer of the galvanized coatings, a 10 vol. % H_2SO_4 solution with Rodine^{TM} 85 inhibitor was used. The stripping procedure comprises the following steps: 1) cover the opposite side of the sample with

electrogalvanizer tape; 2) pour 40ml of the above stripping solution into a beaker; 3) immerse coupon with polymeric pliers; 4) remove the sample when the steel substrate is of uniform appearance after 20 minutes; 5) rinse the sample in deionized water and acetone; 6) pour the stripping solution into a 50ml volumetric flask and dilute to 50ml with 10 vol. % H_2SO_4 solution with Rodine^{TM} 85 inhibitor.

To measure the Al content of the above solution, chemical analysis was performed via ICP (Inductively Coupled Plasma) using matrix-matched standards, i.e. 0.1, 0.5, 1, 5, 10 ppm Al, Fe, Zn reference solution dissolved into10 vol. % H_2SO_4 solution with Rodine^{TM} 85 inhibitor.

3.4.2 Scanning Electron Microscopy (SEM)

To observe the morphology of the Fe-Al interfacial layer, galvanized steel samples were stripped of the Zn overlay using fuming nitric acid via the above procedure and the JSM-7000F field emission scanning electron microscope (SEM) was used to observe the Fe-Al interfacial layer. The operating parameters were set to be 1) acceleration voltage 15keV; 2) working distance 10mm and 4mm. Note that a larger working distance leads to low image resolution but high depth resolution.

To observe any Fe-Zn intermetallic compounds formed when the Al content in the bath was 0.13 wt%, the sample was immersed in a 10 vol% sulphuric acid solution to dissolve

the Zn overlay. After approximately 10 seconds of immersion, three different layers were present on the sample surface from the edge to the center, as shown in Figure 3-6: 1) reflective zinc coating in the centre of the sample; 2) dark grey Fe-Zn intermetallic compounds and Fe-Al compounds in between; 3) light grey layer of Fe substrate in the outer zone.

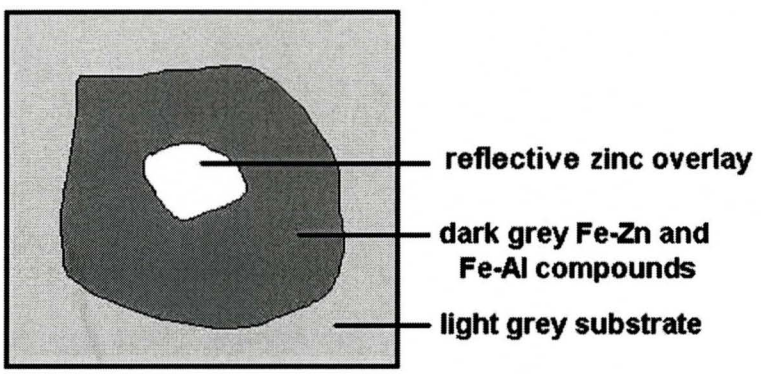

Figure 3-6: Sequence of stripping reactions when using 10% H_2SO_4

3.4.3 Electron Backscatter Diffraction (EBSD)

It is known that as the angle of tilt of specimen surface increases, the interaction volume becomes shallower and smaller. At high stage tilt angles (70° in our case), the electrons can not go very deeply into the sample. It ensures that the depth resolution of the EBSD was quite high and was on the order of 10-100nm [Glodstein, 2003].

Electron Backscatter Diffraction (EBSD) on the JSM-7000F field emission scanning electron microscope was used to identify the intermetallic phases in the interfacial layer and to determine any preferred crystallographic orientation of the Fe-Al interfacial layer. This analysis was performed on samples with the interfacial layer exposed by stripping the zinc overlay using fuming nitric acid. The operating parameters were summarized in Table 3-4. To identify the phases present, the crystallographic parameters of candidate Fe-Al compounds such as structure type, atomic position, atomic occupation and space group were required as input to the computer software for calculation.

Table 3-4: The operating parameters for EBSD

Operating parameter	Value
Acceleration voltage	25 keV
Probe current	medium
Working distance	20mm
Stage tilt angle	70°

CHAPTER 4. RESULTS

4.1 Morphology of the Inhibition Layer

The morphology of the inhibition layer was observed by SEM after the dissolution of the pure zinc overlay with fuming nitric acid, as outlined in the previous chapter.

4.1.1 Influence of Bath Al Content

Figure 4-1 shows the morphology of the inhibition layer obtained when the bath dissolved Al content was 0.1956wt% and the bath temperature was 460°C. It is obvious that there are two types of morphology in the inhibition layer, as previous reported by Baril *et al* [Baril *et al.*, 1999]. Figure 4-2, a high magnification view of Figure 4-1, shows these two sub-layers. Figure 4-2 (a) shows the morphology of the lower sub-layer, which is in contact with the steel substrate. It is a continuous, closely packed layer which consists of small (tens of nanometers), equiaxed Fe-Al intermetallic compound crystals. Figure 4-2 (b) shows the morphology of the upper sub-layer, which is usually (but not always) in contact with the zinc coating. It is comprised of larger (varying in size from 100nm to 800nm), coarse and elongated Fe-Al intermetallic compound crystals among which some small roughly equiaxed crystal are embedded. The two layer morphology of the inhibition layer was observed for all samples when the dissolved Al content in the bath was approximately 0.20wt%, where the bath temperature varied from 450°C to 480°C and the reaction time varied from 2.386s to 5.086s

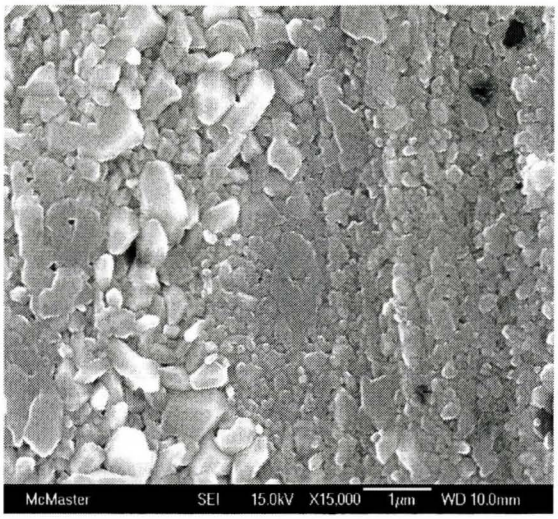

Figure 4-1: Inhibition layer morphology obtained under: dissolved Al content 0.20wt%; reaction time 5.086s; bath temperature 460°C

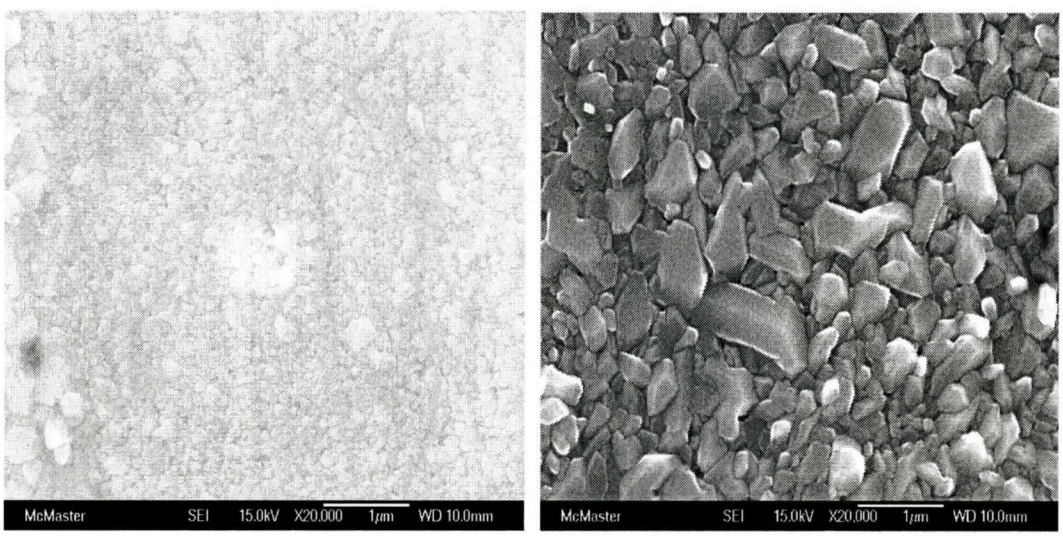

(a) **(b)**

Figure 4-2: Enlargement of the two types of morphology of the inhibition layer obtained under the same conditions as Figure 4-1

However, when the dissolved Al content in the bath was 0.1324wt% at 460°C, it was found that the inhibition layer was incomplete. Figure 4-3 (a) shows the cross-section of a steel panel and Figure 4-3 (b) and (c) show plan view of the morphology of the interfacial layer when the dissolved Al in the bath was 0.1324wt%. In the cross-sectional image, pillar-like Fe-Zn intermetallic compounds were found between the zinc coating and steel substrate. According to the morphology and composition obtained using EDS (Fe: 6.42wt%, Zn: 92.64wt%, Al: 0.93wt %), these Fe-Zn intermetallic compounds were likely ζ-$FeZn_{13}$ phase. From the top view of the inhibition layer surface, it can be seen some bare spots associated with the formation of the Fe-Zn compounds. In this case, the interfacial layer consisted of one layer of small equiaxed grains, as shown in Figure 4-3 (c).

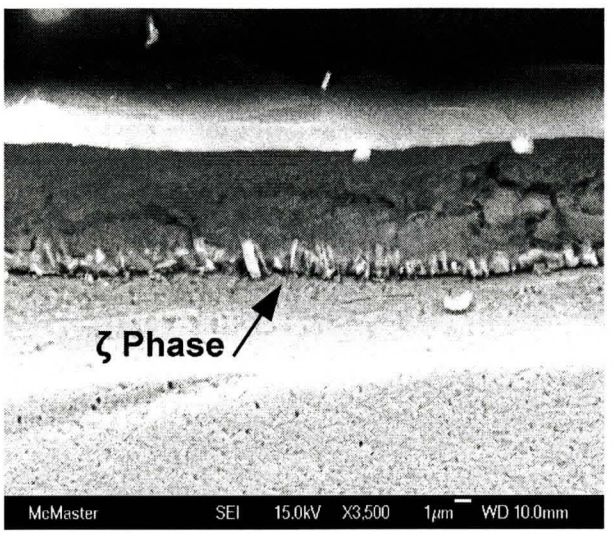

(a)

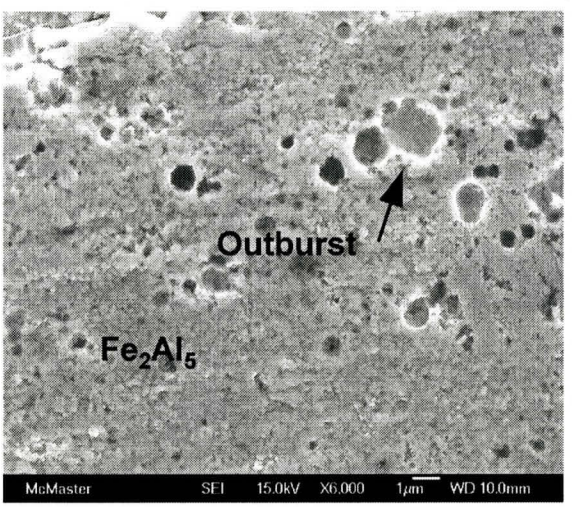

(b)

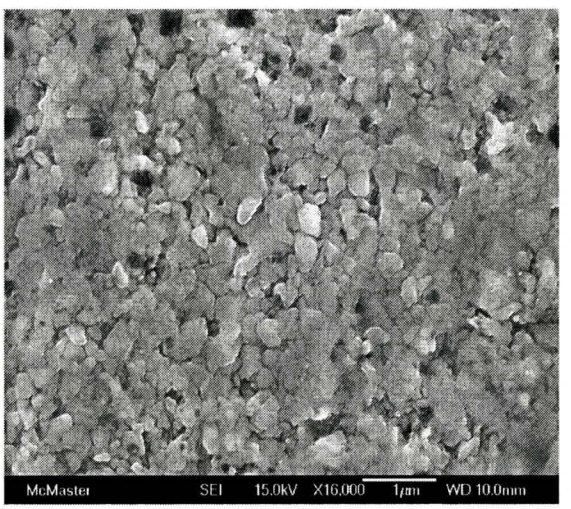

(c)

Figure 4-3: Morphology of the inhibition layer obtained for a dissolved bath Al of 0.13wt%; bath temperature 460°C; reaction time 4.086s. (a) cross-section image of galvanized steel (b) top view of morphology of the inhibition layer (c) enlargement of top view of Fe-Al intermetallic compounds

Figure 4-4 was obtained when the sample coating was stripped using fuming nitric acid. The zinc overlay and Fe/Zn intermetallics were dissolved and the Al-rich interfacial layer was left intact. As can be seen, the inhibition layer was discontinuous, non-compact and was present in isolated islands. The steel substrate was not fully covered by the inhibition layer and the grain boundaries of the steel substrate can be clearly observed. Some substrate grains were not covered by any inhibition layer crystals and the whole grain was exposed to the zinc layer. Some steel substrate grains were partially covered by inhibition layer crystals while the grain boundaries are exposed. Correspondence between Fe-Zn intermetallic compounds and grains boundaries of the steel substrate was observed by Baril *et al* [Baril *et al.*, 1999]. It was revealed by plan-view of the surface of the Fe-Zn compounds in coatings and substrate surface plane-view after dissolution of the Fe-Zn compounds and the inhibition layer in 0.1wt% Al bath with 3.5s immersion time. It was generally accepted and reported that the Fe-Zn intermetallic compounds were preferential formed at the substrate grain boundaries because they were rapid diffusion paths for Zn to diffuse through the interfacial layer [Guttmann *et al.*, 1995; Jordan *et al.*, 1995; Lepretre *et al.*, 1998 (B); Lin *et al.*, 1995 (A)].

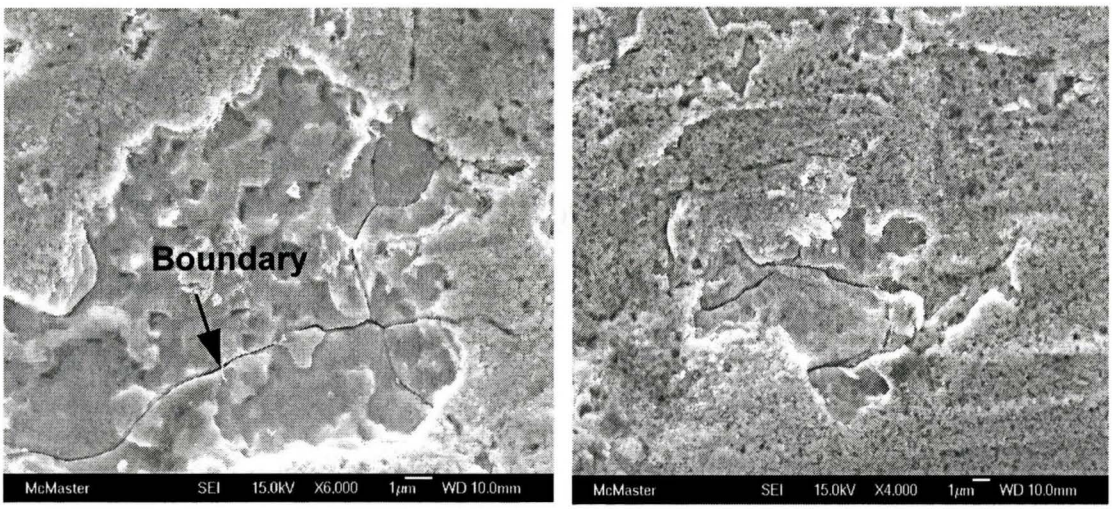

(a)

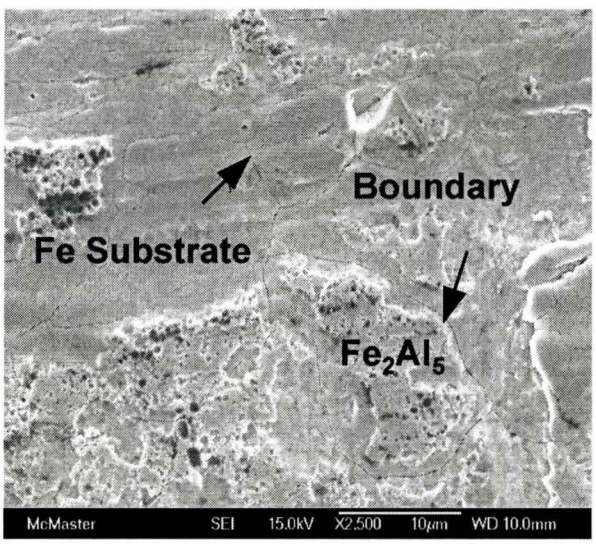

(b)

Figure 4-4: Grains boundaries of the steel substrate when the coatings obtained in 0.13wt% Al bath were dissolved by fuming nitric acid (a) reaction time 3.086s (b) reaction time 4.086s

4.1.2 Influence of Reaction Time

Figure 4-5 shows the inhibition layer morphology when the bath dissolved Al was approximately 0.2wt% for various reaction times. It can be seen that the morphology at 2.186s was the finely crystalline layer next to the substrate and the crystalline layer formed at 7.086s was the randomly oriented upper layer. Also, the number and crystal size of elongated crystals in the upper layer increased with increasing reaction time.

Figure 4-6 shows the inhibition layer morphology when the bath dissolved Al was 0.13wt% but with different reaction times. It can be seen that inhibition layer was not continuous, some Fe-Zn zeta phase outbursts were present and the crystals of the inhibition layer were small and equiaxed. Moreover, with increasing reaction time (from 3.086s to 4.086s), more Fe diffused through the substrate grain boundaries and reacted with Zn, so more zeta phase was observed under the same magnification.

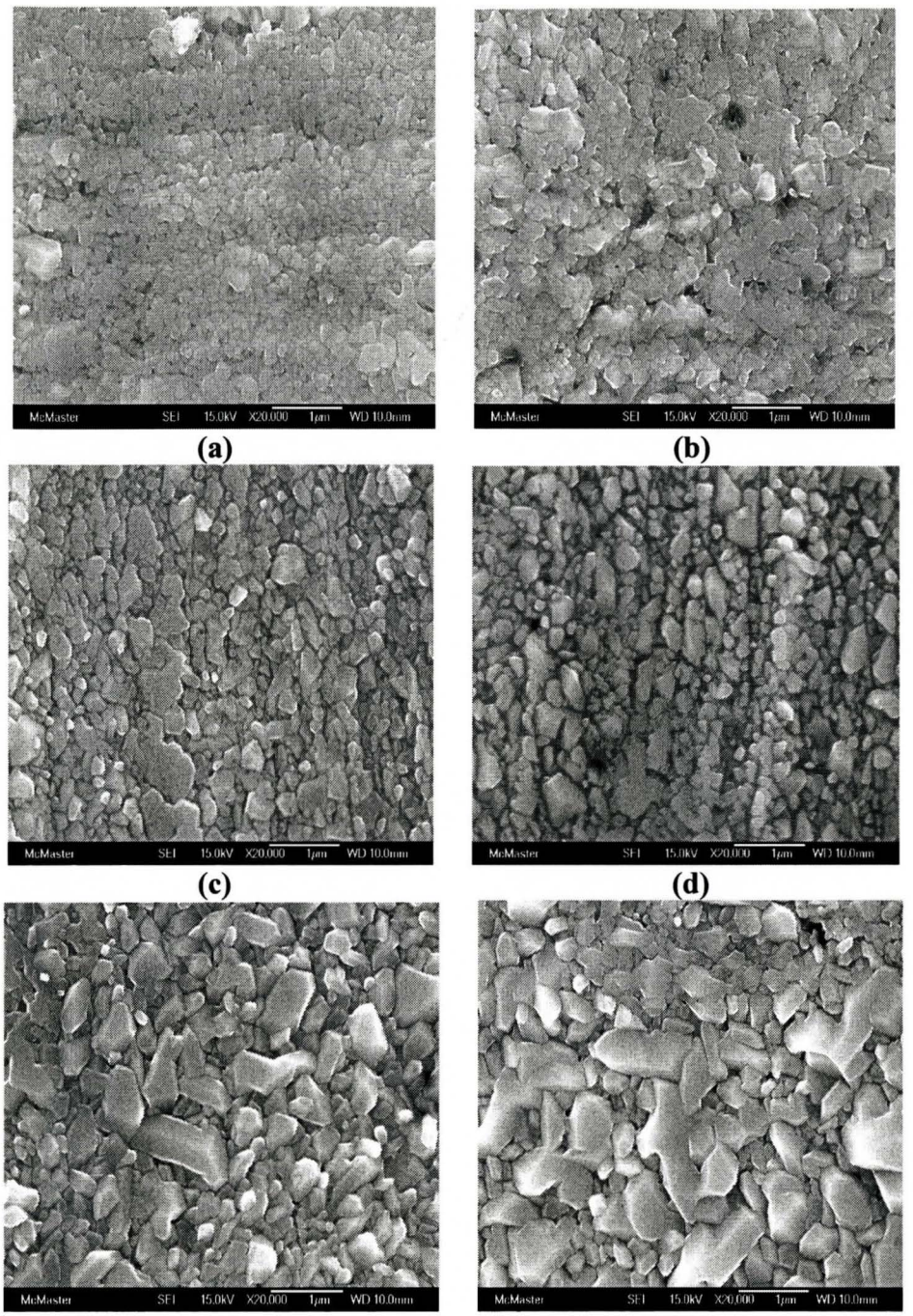

Figure 4-5: Morphology of the inhibition layer obtained for a dissolved bath Al of 0.1956wt%, bath temperature was 460 °C and for different reaction times. (a) 2.186s (b) 2.386s (c) 2.586s (d) 3.086s (e) 5.086s (f) 7.086s

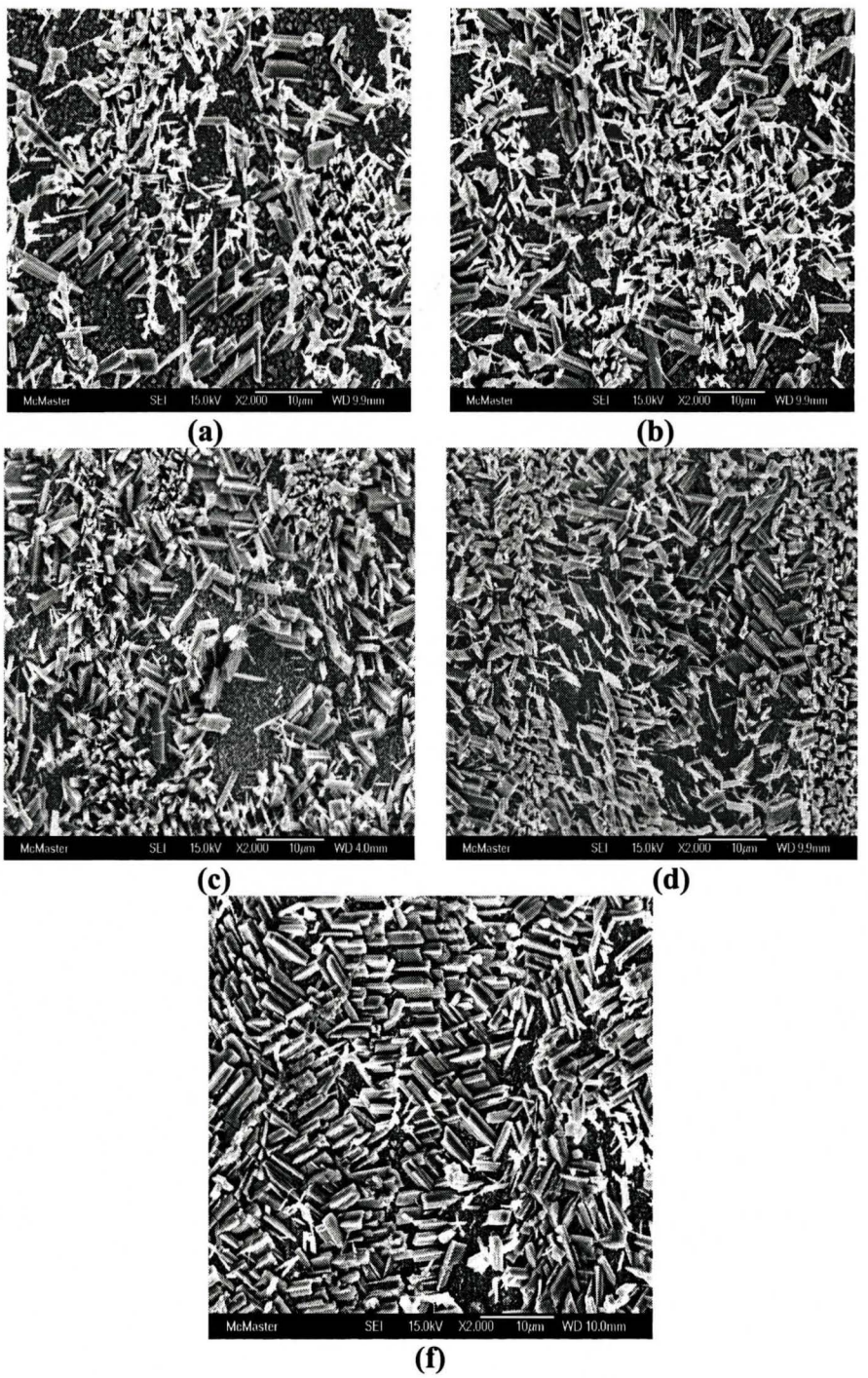

Figure 4-6: Morphology of the interfacial layer for a bath of 0.13wt% dissolved Al as a function of reaction time showing Fe-Zn intermetallic compounds (a) 2.086s (b) 2.586s (c) 3.086s (d) 4.086s (f) 7.086s

4.1.3 Influence of Bath Temperature

The zinc bath temperature is another important parameter during the galvanizing process and has a significant impact on the morphology of the interfacial layer. Figure 4-7 shows the morphology of the inhibition layer obtained with different bath temperatures, from 450°C to 480°C, when the immersion time was 0.1s and the dissolved Al content in the zinc bath was approximately 0.2wt%. From Figure 4-7, it can be seen that for the same immersion time, the inhibition layer structure became coarser at higher temperatures. More large grains were present on the top layer with small equiaxed grains underneath. For the sample at 450°C and 2.076s reaction time (0.1s immersion time), Figure 4-7 (a), the grains were very small and it was difficult to identify the boundaries of grain colonies. With the increasing temperature, it was easier to distinguish even small grains and more faceted coarse grains are observed on the top of lower layer.

As mentioned in literature review, the reason for these morphologies to have appeared for various bath temperatures is that bath temperature has a direct effect on the nucleation and growth kinetics according to classic nucleation and growth theory.

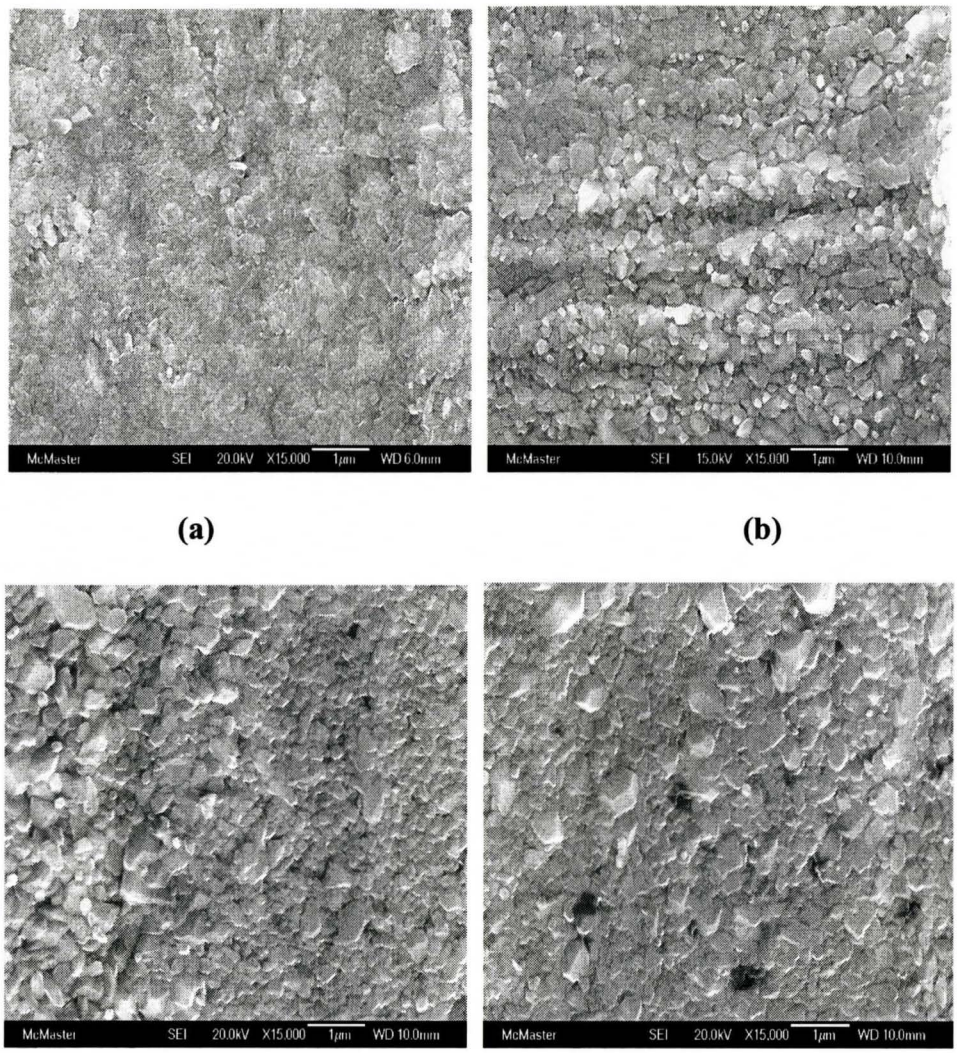

Figure 4-7: Morphology of the inhibition layer obtained with different bath temperature (a) 450°C (b) 460°C (c) 470°C (d) 480°C, immersion time (a) 2.076s (b) 2.186s (c) 2.261s (d) 2.354s and dissolved Al content in the bath was 0.2wt%

4.2 Al Content of the Interfacial Layer

Al is a very important element in the continuous galvanizing process with many different effects on the coating as well as on the zinc bath behaviour [Dubois, 2004]. The total Al of a galvanized coating can be broken down into two parts. One is the Al contained in the zinc overlay, which is related to the dissolved Al content in the zinc bath, but is slightly lower because of post-wiping Al diffusion. The other is the Al uptake in the interfacial layer, which is associated with the formation of Fe-Al intermetallic compounds. In the present study, "Al uptake" is the Al content, in mg/m^2, of the Fe-Al interfacial layer. It is an indirect measure of interfacial layer thickness when there is full coverage of Fe-Al crystals and interfacial layer coverage when there is less than 100% Fe-Al crystals coverage.

4.2.1 Influence of Reaction Time on the Al Content of the Interfacial Layer

The growth kinetics of the interfacial layer, i.e. influence of reaction time on the Al uptake in the interfacial layer, was investigated. Analyses were performed by dissolving the Fe-Al interfacial layer and analyzing for Al using ICP. The influence of reaction time on the interfacial Al uptake is shown in Figure 4-8 and Figure 4-9. The Al uptake in the interfacial layer was found to increase with increasing reaction time for all experimental bath temperatures and for both bath compositions (0.2wt% Al and 0.13wt%Al). Al uptake occurs rapidly. The majority of the Al uptake in the interfacial layer was completed within approximately 2s reaction time (0.1s dipping time). After this time, the

increase of Al uptake in the interfacial layer became more gradual. These results are consistent with the postulated two steps for inhibition layer formation. Nucleation corresponds to a high rate of Al uptake and takes place rapidly. The growth stage is associated with a lower rate of Al uptake.

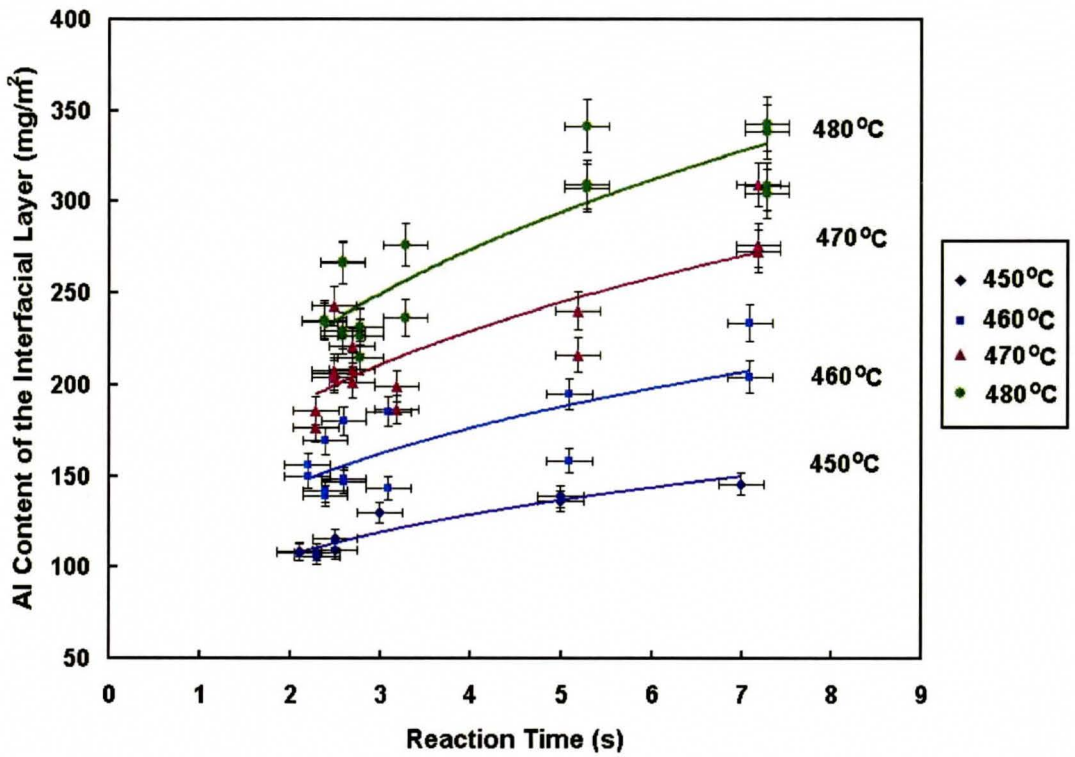

Figure 4-8: Growth kinetics of the interfacial layer in the zinc bath with 0.2 wt% dissolved bath Al for various bath temperatures

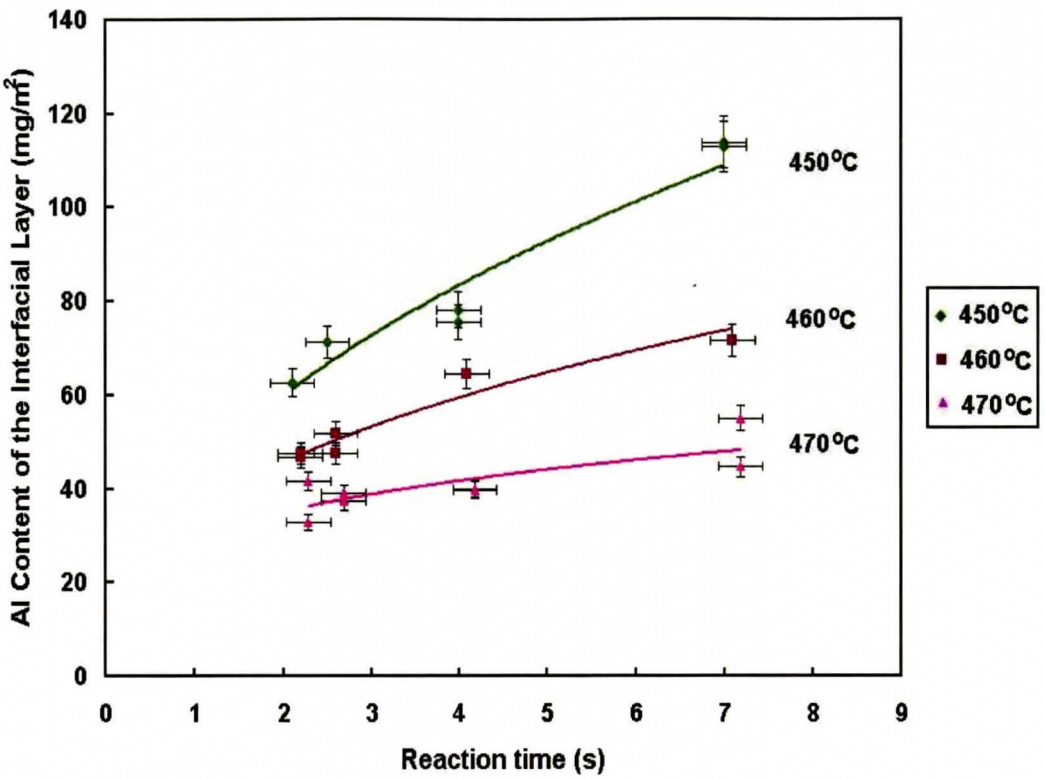

Figure 4-9: Growth kinetics of the interfacial layer in the zinc bath with 0.13 wt% dissolved bath Al for various bath temperatures

From the Figure 4-8, it can be clearly seen that the shortest reaction time between Al and Fe reached was approximately 2 seconds. Comparing the morphology of the inhibition layer obtained in this reaction time, it was found that two-sublayer was observed, which indicates that the full inhibition layer had been formed. So the nucleation kinetics of the Fe-Al interfacial layer reaction were not experimentally captured and only the growth kinetics were studied.

4.2.2 Influence of Bath Temperature and Composition on the Al Content of the Interfacial Layer

When the steel samples were dipped into a bath with 0.2wt% dissolved Al, complete coverage of the interface by the inhibition layer occurred. With increasing bath temperature from 450°C to 480°C, the Al uptake of the interfacial layer increased, as shown in Figure 4-8 and Figure 4-9.

When the steel samples were dipped into the bath with 0.13wt% Al, only a partial inhibition layer was formed and discrete Fe/Zn intermetallic compounds, (ζ phase), were observed. However, as shown in Figure 4-9, the interfacial layer continued to grow during the reaction time. Comparison of Figure 4-8 and Figure 4-9 shows that temperature had the opposite effect on the Al uptake of the interfacial layer in baths with 0.13wt% Al compared to those with 0.2wt% Al, i.e. higher temperatures correspond to lower Al uptake. In addition, the increase in Al uptake with time was minor at higher bath temperatures and was more significant at lower bath temperatures. This observation reveals that the formation of Fe-Zn intermetallic compound is dominant at high temperature due to higher diffusion rate of Fe and Zn at higher bath temperature and that inhibition layer breakdown likely occurs more rapidly. Figure 4-10 shows Fe-Zn intermetallic compounds formed in the zinc bath containing 0.13wt% dissolved Al with different temperatures (from 450°C to 470°C) at the same reaction time. A mixed morphology (Fe_2Al_5- ζ -$FeZn_{13}$ structure) was present because of the inhibition layer

breakdown and growth of ζ phase. In addition, the amount of ζ phase increased with increasing bath temperature.

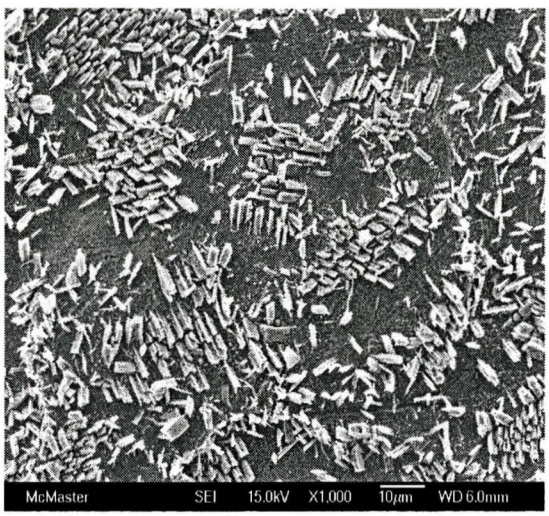

(a)

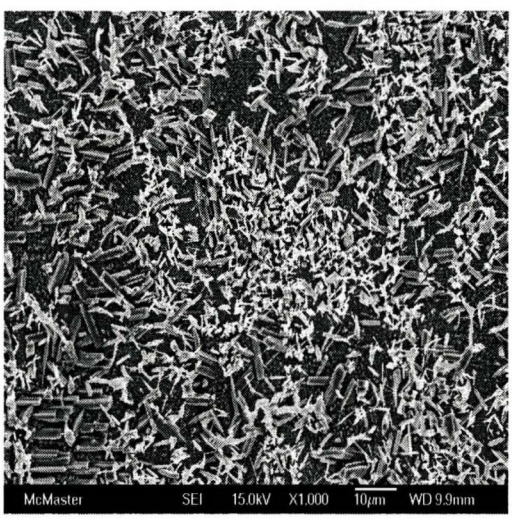

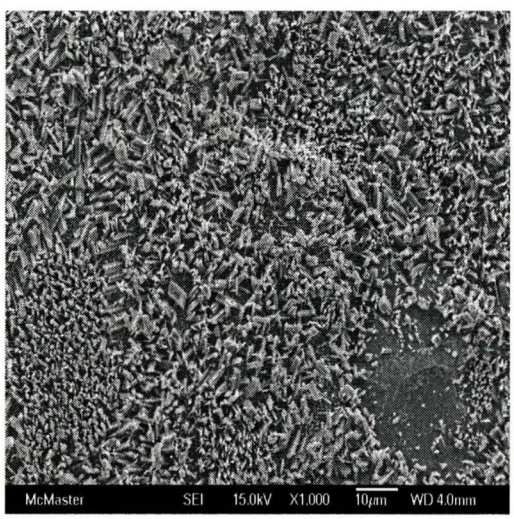

(b) **(c)**

Figure 4-10: Fe-Zn intermetallic compounds formed in the zinc bath containing 0.13wt% dissolved Al with different temperatures (a) 450°C (a) 460°C (a) 470°C (Reaction time were all 4.086s)

4.3 Phase Identification in the Inhibition Layer

Electron Backscatter Diffraction (EBSD) was used to identify the phases present in the Fe-Al inhibition layer and their orientation.

Figure 4-11 and Figure 4-12 show the surface morphology and phase identification for samples with reaction times of 2.186s and 5.086s, respectively, with the same bath temperature of 460°C and dissolved Al content of 0.211wt%. Figure 4-13 shows the Kikuchi diffraction patterns for Fe_2Al_5 and $FeAl_3$. In Figure 4-11 (b) and Figure 4-12 (b), blue represents the Fe_2Al_5 phase, red represents the $FeAl_3$ phase and green represents crystals which could not be identified when the mean angle deviation (MAD) was more than 1.3. In both cases, $FeAl_3$ was identified as being present in the layer. Comparing the SEM images with that of the phase maps in Figure 4-12, it seems that the Fe_2Al_5 phase corresponds to the particles sticking out of the surface and the coarse crystals of the upper layer. Conversely, $FeAl_3$ corresponds to the fine crystals of the lower layer. The phase map in Figure 4-11 was obtained when the surface of the galvanized steel sample was slightly polished in order to obtain a stronger and clearer diffraction pattern due to the thinner inhibition layer formed in the short reaction time. In this figure, more $FeAl_3$ crystals, (red), were observed versus Fe_2Al_5, (blue). For longer reaction times (Figure 4-12), this balance is shifted towards a larger proportion of Fe_2Al_5. However, it was not possible to quantify the relative proportions of these two phases because of many areas of missing data. The possible reasons for this are: 1) EBSD is a surface-sensitive technique, with the diffraction signal coming from the top few nanometers of the crystal lattice.

Thus, high quality sample preparation is essential to obtain a strong and clear electron backscatter diffraction pattern (EBSP). If the sample surface was not mirror flat, the EBSPs will appear very weak and blurred [HKL-Technology, 2006] and result in large areas of missing data, (green). 2) The crystallographic information for Fe_2Al_5 and $FeAl_3$ phases was required for the software to work properly. However, these two phases could actually be Zn bearing Fe-Al phases according to the literature [Chen *et al.*, 1990 (A)]. Some crystallographic parameters may have deviated from the data used in assessing the diffraction patterns, which would have resulted in a high MAD value and increase the amount of non-evaluated points.

According to the pole figure obtained for both phases, Figure 4-14, it was found that both the Fe_2Al_5 and $FeAl_3$ crystals exhibited strong preferred crystallographic orientations. This conclusion was drawn based on the observation that the normal of the (100) planes had an extremely high intensity in a direction approximately normal to the substrate surface for both intermetallics.

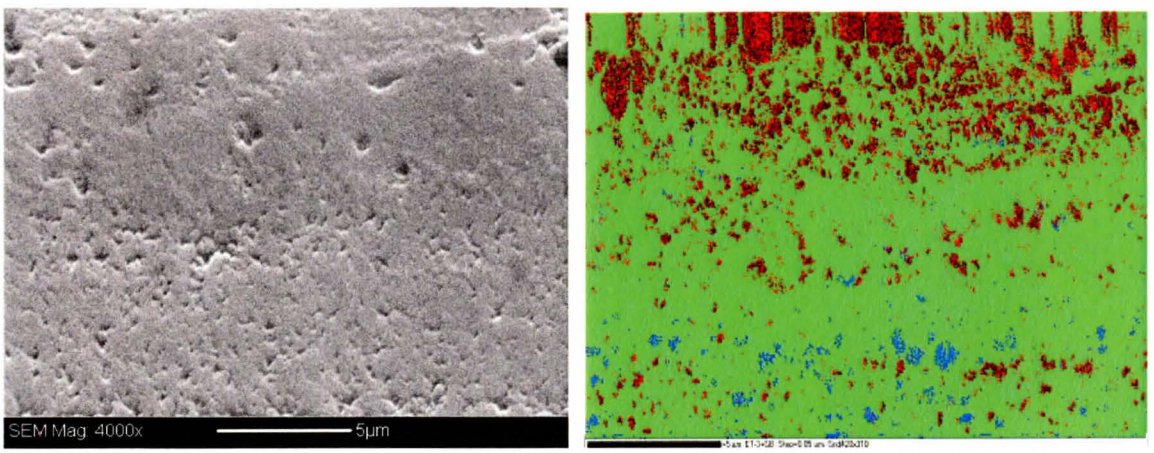

(a) (b)

Figure 4-11: Surface morphology and phase identification for polished sample obtained for a reaction time of 2.186s; bath temperature was 460°C; bath dissolved Al content was 0.211wt% (a) surface image (b) phase map

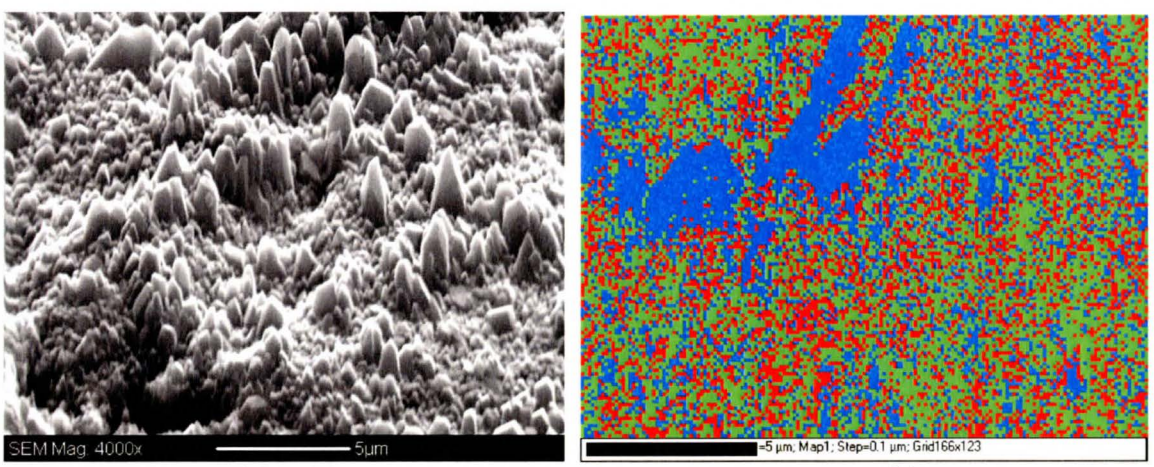

(a) (b)

Figure 4-12: Surface morphology and phase identification for sample obtained for a reaction time of 5.086s; bath temperature was 460°C; bath dissolved Al content was 0.211wt% (a) surface image (b) phase map

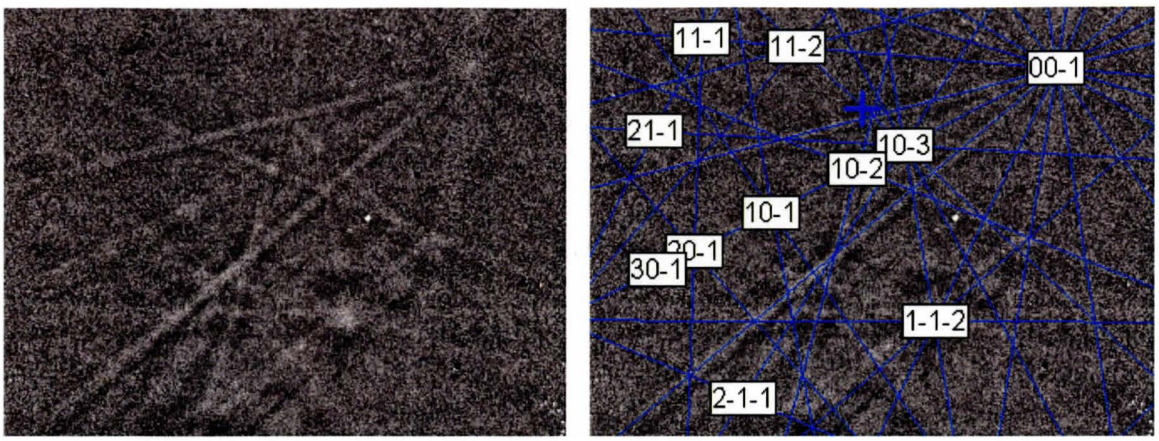

(a)

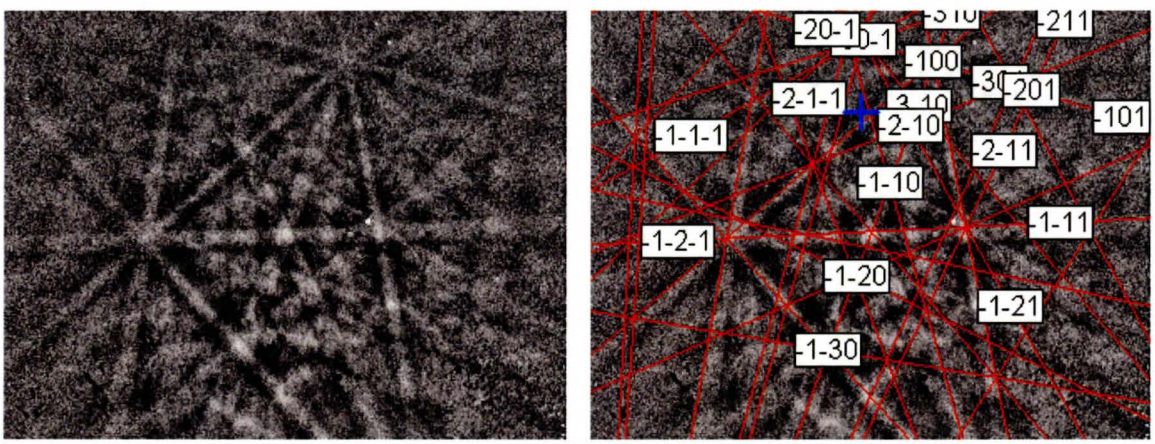

(b)

Figure 4-13: Kikuchi diffraction patterns for (a) Fe_2Al_5 (b) $FeAl_3$

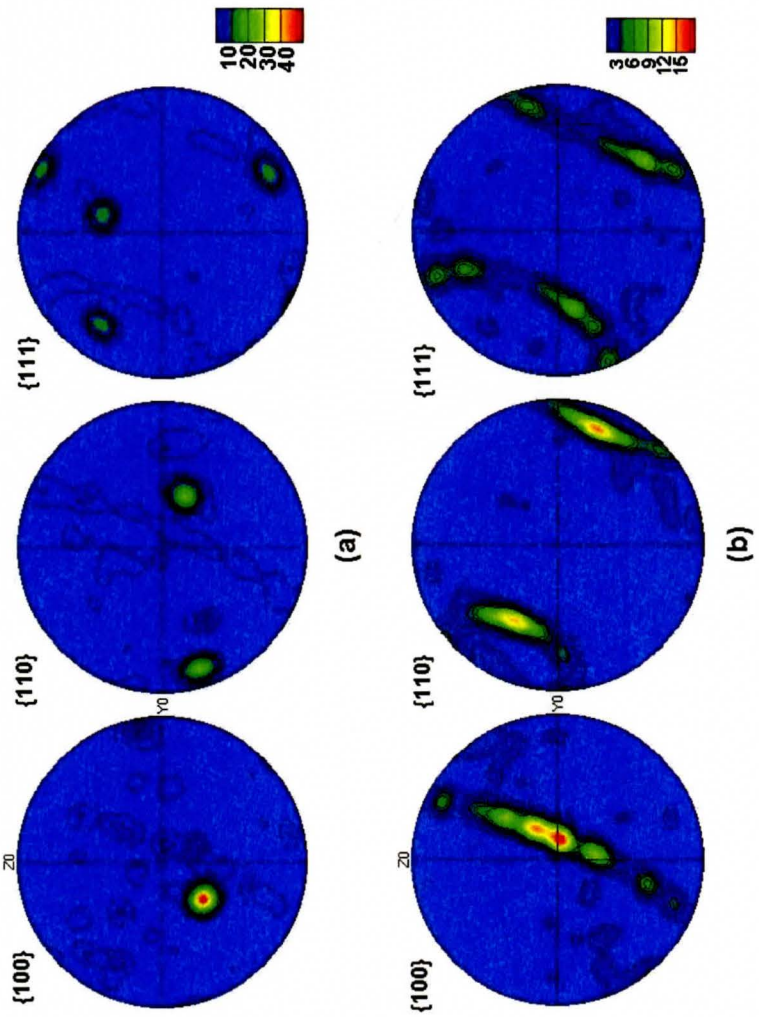

Figure 4-14: Pole figures shown the preferred orientations for samples obtained for a reaction time of 5.086s; bath temperature was 460°C; bath dissolved Al content was 0.211wt% (a) Fe_2Al_5 (b) $FeAl_3$

CHAPTER 5. DISCUSSION

Reaction time is a crucial parameter in studying the evolution and kinetics of inhibition layer formation during hot-dip galvanizing. Many researchers have made an effort to investigate this process. It is believed that the inhibition layer is nucleated at very short times (i.e. less than one second). However, it has been mentioned previously that the mechanism of short time inhibition layer formation has been studied by only a few people due to experimental difficulties. Moreover, only short immersion times (i.e. dipping time), not total reaction time, has been examined by many investigators. It was generally found that the Al content in the zinc coating, excluding the Fe-Al interfacial layer, is always lower than the dissolved Al content in the zinc bath because of Al diffusion after wiping to the interfacial layer [Dubois *et al.*, 1993] [Faderl *et al.*, 1995] [Baril *et al.*, 1998] [Dubois, 2004]. Thus, the Al uptake still increased, i.e. the Fe-Al interfacial layer kept growing, after the steel sheet was withdrawn from the zinc bath. Thus, it is the opinion of author that the use of immersion time instead of total reaction time to describe the kinetics of the inhibition layer formation is not correct. Thus, one significant aim of this project was to study the characteristics, such as morphology, phase constitution and kinetics, of inhibition layer formation based on a well defined reaction time which includes the dipping time, the time between exiting the zinc bath and the time before solidification of the overlay. As outlined in the previous chapter, the inhibition layer was characterized by using the combined methods of SEM, ICP and EBSD.

5.1 Characteristics of the Inhibition Layer Formed in a Bath with 0.2wt% Dissolved Al

5.1.1 Formation Kinetics

In the present study, wet chemical analysis (ICP) combined with the total reaction time calculation was used to investigate the kinetics of inhibition layer formation. This represents the first known work in which the Al uptake in the interfacial layer has been established based on actual reaction time. This work has practical significance. It has been shown that a mass balance model of the hot-dip galvanizing bath could be used to monitor the bath effective Al, predict future bath additions and benchmark the performance of the continuous galvanizing line, particularly dross production [McDermid *et al*, 2004 (A)]. However, it is impossible to build good models of the reactions inside the continuous galvanizing line (i.e. mass balance during the galvanizing process) without a good kinetic model of Al uptake to the substrate as a function of the various process parameters. Also, it actually gives us a chance to have a glimpse at the structure of the interfacial layer in the bath as a function of real time by freezing the structure at various reaction times. "Frozen pictures" of the reaction in the zinc bath were seen through this work, which has not been done before.

According to the observations of the morphology of the inhibition layer, as shown in Figure 4-1 and Figure 4-5, it was found that the inhibition layer was formed with a layered structure for all experimental temperatures and times when the zinc bath

contained 0.2 wt% dissolved Al. The lower layer was composed of small, roughly equiaxed, closed packed crystals. The upper layer consisted of larger, coarser crystals. These observations were in agreement with previous reports by Guttmann *et al* and Baril *et al* [Guttmann *et al.*, 1995] [Baril *et al.*, 1999]. Moreover, the observed morphology of the inhibition layer can help explain the reaction kinetics obtained through ICP analysis and total reaction time calculation. According to Figure 4-8, it was revealed that the majority of Al uptake was completed within a reaction time of 2 seconds (i.e. 0.1s dipping time). The subsequent Al uptake can be approximately characterized as following a parabolic rate law, indicating diffusion controlled growth.

Accordingly, the formation sequence for the inhibition layer can be summarized as follows:

(1) in the first period, Fe-Al intermetallic compounds nucleate on the surface of the steel substrate and grow until the surface is completely covered with one layer of crystals which are small and roughly equiaxed. The majority of the Al uptake is completed within this period. (2) in the second period, this layer grows by Al provided from the Al-bearing zinc bath and Fe from the steel substrate diffusing through the inhibition layer grain boundaries. This growth follows a parabolic growth law, to be discussed below, typical of diffusion controlled growth.

In order to explore the shortest period of the Fe-Al reaction in the Al-bearing zinc bath, short dipping times (as shortest as 0.1s) and rapid helium cooling (fastest cooling rate

was 108 °C/s) technologies were used. However, despite these efforts, the shortest reaction time between Al and Fe achieved in the present study was approximately 2s. From the morphology of the inhibition layer obtained in this reaction time, it was found that the inhibition layer had been completely formed. Thus, the nucleation kinetics of the Fe-Al interfacial layer reaction could not be experimentally examined due to the limitations of the present apparatus. Only the growth kinetics was captured. Also, the existence of an incubation time, i.e. the time taken for Fe to dissolve into zinc bath to reach a local supersaturation in the vicinity of the surface of the steel sheet, immediately following immersion and prior to nucleation, could not be determined.

5.1.2 Microstructure of the Inhibition Layer

It has been widely accepted that the inhibition layer was composed of Zn-bearing Fe_2Al_5 phase [Harvey *et al.*, 1973] [Faderl *et al.*, 1992] [Saito *et al.*, 1991] [Tang *et al.*, 1993] [Guttmann *et al.*, 1995] [Price *et al.*, 1999] [Baril *et al.*, 1999]. In the present study, EBSD was used to determine that two phases, Fe_2Al_5 and $FeAl_3$, coexist in the Fe-Al inhibition layer, as shown in Figure 4-11 and Figure 4-12. Furthermore, the EBSD observations suggest that reaction time has an influence on the phase constitution of the inhibition layer. For the shorter reaction times (i.e. 2.186s), the majority of the phases detected were $FeAl_3$, as shown in Figure 4-12 (b). This indicates that $FeAl_3$ was the first phase present on the surface of steel substrate. With further development of the inhibition layer, more Fe_2Al_5 crystals were observed. In addition, comparing the SEM image and that of the phase map in Figure 4-11, it was determined that the Fe_2Al_5 phase

corresponded to the coarse particles on the upper layer and $FeAl_3$ phase was associated with the fine particles in the lower interfacial layer. It appears that Fe_2Al_5 has grown out to form the upper coarse layer by transforming from $FeAl_3$. Both Fe_2Al_5 and $FeAl_3$ have a preferred growth orientation. These observations were consistent with previous report that for very short times transient phases with a composition around $ZnFeAl_3$ were formed [Ghuman *et al.*, 1971] [Perrot *et al.*, 1992].

McDevitt *et al* [McDevitt *et al.*, 1997] and Morimoto *et al* [Morimoto *et al.*, 1997] proposed two possible mechanisms for the formation of the layered microstructure of the inhibition layer. The first proposed that Fe_2Al_5 first nucleates on the steel substrate, followed by nucleation and growth of $FeAl_3$ on the surface of the existing Fe_2Al_5 layer. The second was that $FeAl_3$ first nucleates on the steel substrate, followed by nucleation and growth of Fe_2Al_5 at the interface of the steel substrate and the $FeAl_3$ phase. Based on the EBSD results presented above, it appears that the sequence occurring during the development of the inhibition layer was most likely the second possibility, i.e. (1) $FeAl_3$ first nucleates on the steel substrate; (2) $FeAl_3$ phase transforms to Fe_2Al_5 phase through a diffusion mechanism; (3) $FeAl_3$ phase continues to diffusively transform to Fe_2Al_5 phase and Fe_2Al_5 phase starts to grow a two sublayer structure, i.e. formation of the coarse upper large of Fe_2Al_5 crystals; (4) $FeAl_3$ phase disappears and the two layer structure of the interfacial layer is composed of Fe_2Al_5 crystals. This process is schematically illustrated in Figure 5-1.

According to the Zn-Fe-Al ternary phase diagram (Figure 2-6) [Perrot *et al.*, 1992], there is thermodynamic equilibrium between α-Fe and Fe_2Al_5, whereas $FeAl_3$ is not in equilibrium with α-Fe. However, $FeAl_3$ crystals were actually observed using EBSD in the case of a 0.2 wt% dissolved Al bath at 460°C when the reaction time varied from 2.186s to 5.086s (i.e. dipping time from 0.1s to 3s). This indicates that $FeAl_3$ was in metastable state. Consequently, it only appeared in the first stage of the process of Fe-Al compound formation and then diffusively transformed to the thermodynamic equilibrium phase, i.e. Fe_2Al_5 phase.

When the steel sheet entered the zinc bath with 0.2wt% dissolved Al, the steel sheet zinc bath interface was obviously out of equilibrium, which resulted in the dissolution of Fe into liquid zinc to reach a local supersaturation with Fe in the vicinity of the Fe/Zn interface. However, equilibrium of the zinc bath had to be finally satisfied, so this supersaturation leads to the formation of a continuous layer on the steel surface in equilibrium with zinc bath [Lepretre *et al.*, 1998 (B)]. Due to the much lower formation free energy (as shown in Table 2-1), Fe-Al compounds favourably nucleated on the steel surface instead of Fe-Zn intermetallic compounds. At the first moment of this process, the Al content in the zinc bath was enough to allow the nucleation of the metastable Fe-Al phase, i.e. $FeAl_3$. As it is known that the Al content of the interfacial layer is much higher than the Al content of the zinc bath, formation of Fe-Al interfacial layer ($FeAl_3$) would lead to a Al depletion in the vicinity of the interfacial layer surface. In consequence, a metastable Fe-Al phase with higher Al content, $FeAl_3$, would transform to

the equilibrium Fe-Al phase with a lower Al content, Fe_2Al_5, by a diffusive reaction, as shown in equation 5-1.

$$FeAl_3 + 2Al(bath) + Fe(substrate) + xZn(bath) \rightarrow Fe_2Al_{5-x}Zn_x \quad (5\text{-}1)$$

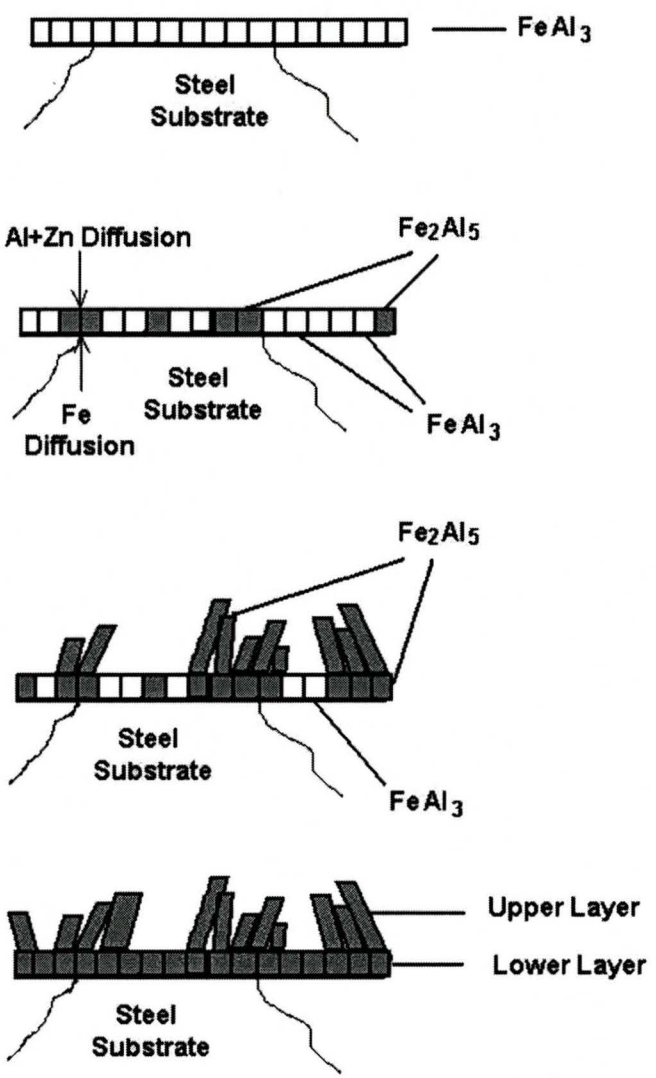

Figure 5-1: Schematic representation of the inhibition layer formation in a 0.2wt%Al-Zn galvanizing bath

It has been mentioned previously that the structure and composition of the inhibition layer was studied by many galvanizing researchers. They investigated the inhibition layer using different analytic methods, such as SEM, EDS, XRD, TEM, and often yielded conflicting results. Only the Zn-bearing Fe_2Al_5 phase was observed by most of them. They failed to identify the $FeAl_3$ phase. There may be several reasons for the observation of the $FeAl_3$ phase in the present study versus the observations of many previous researchers: (1) reaction time: it has been shown that $FeAl_3$ is the phase which appears in the early stages of inhibition layer formation. Thus, any experiments using either long immersion times or slow cooling after immersion will likely miss the transient stage where $FeAl_3$ in present and (2) analytical technology: the poor signal to background ratio combined with the small volume fraction of $FeAl_3$ phase results in $FeAl_3$ being undetectable [McDevitt *et al.*, 1997] by regular X-ray diffraction.

5.2 Characteristics of the Inhibition Layer Formed in a Bath with 0.13wt% Dissolved Al

The experimental results showed that when the zinc bath contains 0.13wt% dissolved Al, there were intermittent patches of Fe-Zn intermetallic compounds, identified as ζ phase, within the inhibition layer. There is general agreement on the mechanism of Fe-Zn intermetallic compounds formation. First, Zn diffuses through the Fe_2Al_5 layer and saturates the substrate, particularly at the grain boundaries. Fe-Zn intermetallic

compounds nucleate at the Fe- $Fe_2Al_5/FeAl_3$ interface, destroying the overlying inhibition layer. Fe-Zn intermetallic compounds then grow along the interface from the grain boundaries and gradually consume the Fe_2Al_5 layer [Baril *et al.*, 1998].

McDevitt *et al* [McDevitt *et al.*, 1998] reported that these Fe-Zn intermetallic compounds nucleated on the top of the Fe-Al layer from the Fe-supersaturated liquid Zn. However, the results presented in Figure 4-4 show that the steel substrate was not fully covered by the inhibition layer and the grain boundaries of the steel substrate can be clearly observed. Correspondence between Fe-Zn intermetallic compounds and grains boundaries of the steel substrate was observed by Baril *et al* [Baril *et al.*, 1999]. This result indicates that Fe-Zn intermetallic compounds nucleated at the grain boundaries of the steel substrate, which is the short circuit diffusion path and results in higher zinc concentration at these sites [Lepretre *et al.*, 1998 (B)].

It was not clear whether the Fe-Zn compounds form during isothermal holding in the bath [McDevitt *et al.*, 1998] or after exiting [Baril *et al.*, 1998] [Guttmann *et al.*, 1995]. Figure 4-6 showed Fe-Zn intermetallic compounds, pillar-like ζ, present on the steel substrate surface when zinc bath contains 0.13% dissolved Al at 460°C for all reaction times studied. It was revealed that more Fe-Zn compounds were present in the structure with increasing reaction time. In addition, ICP results indicated that that the Al content of the interfacial layer continued to increase with reaction time for baths with 0.13wt%Al, as shown in Figure 4-9, indicating that Fe-Al compounds continue to grow during this

period. It was therefore quite likely that an Fe-Al interfacial layer forms on the steel substrate in the very early stages, after which zinc diffuses through the Fe-Al layer via the Fe-Al compound grain boundaries to react with Fe, which results in initiation of inhibition breakdown and Fe-Zn intermetallic compound formation.

Guttmann [Guttmann *et al.*, 1995] provided a rough estimate of the average diffusion coefficient for Zn through the Fe-Al layer of $5\times10^{-11} cm^2 \cdot s^{-1}$. This value implies that Zn could diffuse across a 70nm thick Fe-Al layer in 1s and a 250 nm layer in 3s at 460°C. Longer immersion time correspond to more Fe-Zn intermetallic compound formation due to greater masses of zinc diffusing through the Fe-Al interfacial layer. After samples exited the zinc bath, Fe-Al reaction slows down due to a limited Al supply from the Zinc overlay. Fe-Zn intermetallic compounds continuously grow by consuming the Fe-Al layer.

From the discussion above, it seems that the evolution of the interfacial layer formed in a zinc bath with 0.13wt% dissolved Al, including Fe-Al and Fe-Zn intermetallic compounds, was the result of competing reactions, i.e. the Al uptake of the Fe-Al interfacial layer increased during the reaction period, as shown in Figure 4-9, and there were increasing amounts of ζ-$FeZn_{13}$ with increasing reaction time, as shown in Figure 4-6. These results can be explained as follows:

(1) In the initial period, Fe-Al formation dominates due to favourable thermodynamics. This is demonstrated in Figure 5-2, which shows the driving force for nucleation of

various Fe-Al and Fe-Zn phases from a supersaturated Zn-Fe-Al solution [Nakano, 2006]. Thus, Fe from the steel moves towards the zinc bath through the interfacial layer and combines with Al in the bath to form and growth Fe-Al layer; at the same time, zinc diffuses from the zinc bath towards the steel substrate, thus enriching the α-Fe/Fe_2Al_5 interface with zinc [Lepretre *et al.*, 1998 (B)]

(2) After the zinc content in the substrate reaches the critical content, needed to form Fe-Zn compounds according to the phase diagram, initiating inhibition breakdown and the growth of Fe-Zn reaction dominates. Therefore, the increase in Fe-Al compounds while observing increasing amounts of ζ-$FeZn_{13}$ reveals that there is competition between these two reactions. Fe-Al compound is favoured by thermodynamic driving forces and formation of ζ-$FeZn_{13}$ (or other Fe-Zn intermetallic compounds) is kinetically favoured by other factors, namely the diffusion of Zn through the Fe-Al layer and saturation of the substrate.

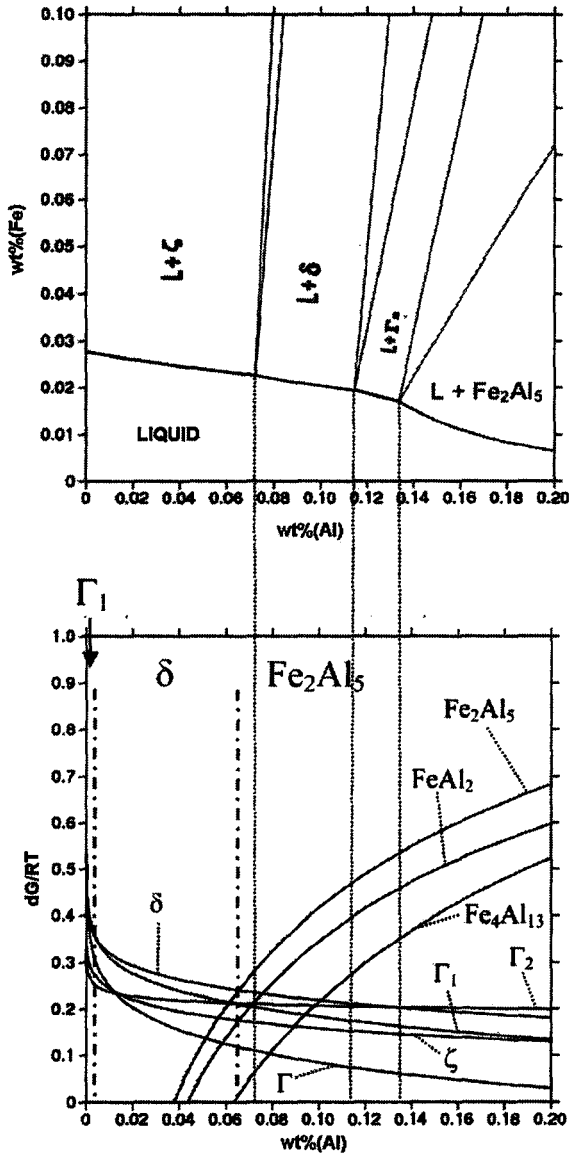

Figure 5-2: Driving force for nucleation at 450°C in Zn-Fe-Al (assuming that Fe is dissolved in the liquid at the interface to the metastable solubility limit as in Figure 2-5) [Nakano, 2006]

Bath temperature also has influence on the competition between Fe-Al and Fe-Zn compounds. Figure 4-8 shows that the growth of Fe-Al intermetallics increases with increasing bath temperature. On the other hand, diffusion of Zn and Fe through the Fe-Al

layer is also enhanced with increasing temperature. As a consequence, Fe-Zn growth became dominant in the competition with Fe-Al reaction. Figure 4-10 shows the experimental evidence for this statement. More Fe-Zn intermetallic compounds were observed when the bath temperature varied from 450°C to 480°C with the same reaction time, decreasing the Al content of the interfacial layer with increasing bath temperatures, as shown in Figure 4-9.

5.3 Kinetic Model of Inhibition Layer Formation (0.2wt% Al Bath)

It has been previously mentioned that the initial formation period of the inhibition layer, including any incubation period and nucleation, was not experimentally observed in the present study. However, the nucleation time can be predicted based on the Al uptake during the growth period as function of the total reaction time through a kinetic model.

Figure 4-8 showed the Al uptake of the interfacial layer in a zinc bath with 0.2 wt% dissolved Al for various bath temperatures based on reaction time. Comparing these data to those provided by Toussaint *et al* in Figure 5-3 [Toussaint *et al.*, 1998 (B)], it is interesting to note that the values of Al uptake in their experiments were higher than those in the present work. It should be noted that the data for the experiments in the current study have been re-plotted as a function of immersion time for the purpose of comparison. For instance, in their study, the interfacial Al content was approximately 250mg·m^{-2} for an immersion time of 1s when the bath temperature was 460°C and 0.2wt%Al in the zinc bath. However, approximately 170mg·m^{-2} Al was obtained in the present experiments with the same experimental parameters. This difference likely arises from the different cooling rates after the steel samples exited the zinc bath, i.e. differences in post immersion Al diffusion to the interface.

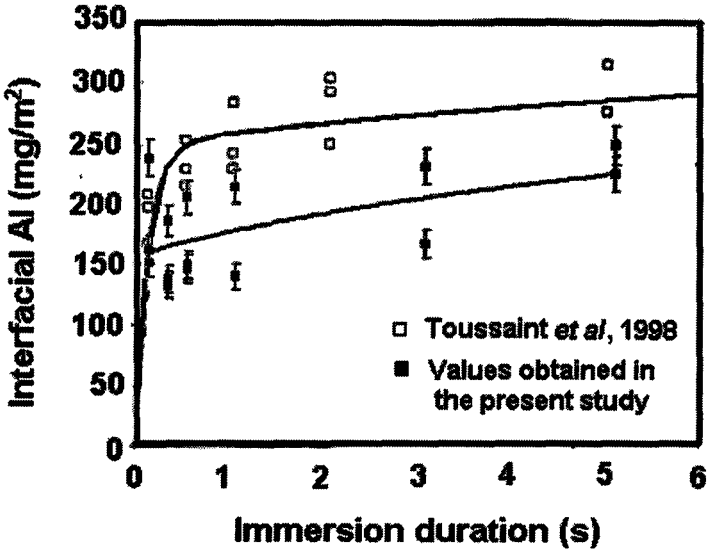

Figure 5-3: Experimental points for the Al uptake form Toussaint *et al* [Toussaint *et al.*, 1998 (A)] and this study

It has been generally accepted that the formation of the inhibition layer is a two-stage process [Isobe, 1992; Tang, 1995 (A); Toussaint *et al.*, 1998 (C)]. Nucleation is almost instantaneous, associated with a high rate of Al uptake, which stops when the substrate is completely covered. The following step corresponds to solid state diffusional growth, associated with a lower rate of Al uptake. Diffusional growth will be dominant when nucleation is completed.

Solid-state diffusion growth will be discussed in the following text. The growth rate index, n, was taken into consideration in this study. A power-law growth equation, as shown in equation 5-2, may be used to fit the growth kinetics data (Figure 4-8) such that:

$$Y = K \cdot t^n \tag{5-2}$$

where Y is the Al uptake of the interfacial layer in mg/m^2, K is the growth rate constant; t is the reaction time and n is the growth-rate time constant. The growth-rate time constant, n, is an indication of the mechanism controlling the growth of the layer [Jordan *et al.*, 1997(A)]. When n is equal to 0.5, the layer exhibits bulk diffusion controlled growth; while a n value of 0.25 indicates grain boundary diffusion controlled growth. By fitting an equation for the data shown in Figure 4-8, it was found that the curves of the form $y = K \cdot x^n$ fit the present experimental points very well. The range of the value for growth-rate time constant, n, was 0.27 for the interfacial layer growth at 450°C and was equal to 0.31 for the 480°C bath, as shown in Table 5-1. This may indicate that nucleation phenomena play an important part in the overall kinetics [Toussaint *et al.*, 1998 (C)]. A value of n between 0.25 and 0.5 may also indicate a mixed growth mechanism of bulk diffusion and grain boundary diffusion for this interfacial layer.

Table 5-1: Growth constant for experimental fitting

T	K	n
450°C	88.48	0.27
460°C	118.54	0.28
470°C	153.14	0.29
480°C	175.45	0.31

For the diffusive growth stage, both lattice (or bulk) diffusion and grain boundary (or short circuit) diffusion likely contribute to the overall growth rate. In general, grain boundary diffusion is dependent on the grain boundary area. The influence of reaction time and bath temperature on the morphology of the inhibition layer was investigated in

this study. It was found that the inhibition layer was composed of many small equiaxed crystallites and the average size of the crystallites increased as the inhibition layer thickened, as shown in Figure 4-5. In addition, the crystallites of the inhibition layer became coarser for the same reaction time at higher bath temperatures, as shown in Figure 4-7. Thus, the conclusion may be drawn that the mean size of crystallites in the inhibition layer increased in size both as a function of reaction time and bath temperature.

From the results of grain size measurement, it can be demonstrated that the development of the inhibition layer structure plays an important role in the growth kinetics. First, as the reaction proceeded, the mean size of the crystallites increased and the area fraction of grain boundaries decreased. Thus, the effect and contribution of lattice diffusion became more dominant. Second, grain boundary diffusion generally becomes increasingly important with decreasing temperature. There are two reasons for this. One is that the activation energy for grain boundary diffusion is smaller than that for lattice diffusion. The other one is that, for a given reaction time, the grain size of the inhibition layer generally becomes smaller the lower the temperature and thus, had a higher area fraction of grain boundaries [Kofstad, 1988].

Several models for oxide film growth have been proposed based on the assumption that the kinetics are a combination of both lattice and grain boundary diffusion [Herchl *et al.*, 1972; Kofstad, 1988; Perrow *et al.*, 1968; Perrow *et al.*, 1967]. Based on this assumption,

an effective diffusion coefficient (D_{eff}) may be defined as a weighted sum of lattice and grain boundary diffusion:

$$D_{eff} = D_L(1-f)+D_B f \tag{5-3}$$

Where D_L and D_B are diffusion coefficients for the lattice and grain boundary, respectively, and f is the area fraction of grain boundaries. In the model advanced by Smeltzer *et al* [Smeltzer *et al.*, 1961], the fraction of available diffusion sites within the grain boundaries decreased according to the first-order kinetic equation:

$$f(t) = f^0 \exp(-Kt) \tag{5-4}$$

where, f^0 is the initial fraction of total grain boundaries and K is the growth constant. The rate of film growth based upon the diffusion gradient would then be:

$$\frac{dx}{dt} = \Omega D_{eff} \frac{\Delta c}{x} \tag{5-5}$$

Using the growth of oxide films as an analogy for the growth of the inhibition layer, the terms in equation (5-5) can be defined as: x is the inhibition layer thickness, Ω is the volume per Fe ion in the inhibition layer (cm^3 per ion) and Δc is the concentration difference of Fe ions at the two surfaces of the inhibition layer (ions per cm^3). The value for Δc suggested by Toussaint *et al* [Toussaint *et al.*, 1998 (C)] was estimated to be approximately $50\times10^6 mg\cdot m^{-3}$. Substitution of equations (5-3) and (5-4) into equation (5-5), yields:

$$\frac{dx}{dt} = \Omega\left\{D_L\left(1-f^o e^{-Kt}\right)+D_B f^0 e^{-Kt}\right\}\frac{\Delta c}{x} \tag{5-6}$$

Using the approximation that $D_B \rangle\rangle D_L$, equation (5-6) becomes:

$$x\frac{dx}{dt} = \Omega D_L \Delta c\left\{1 + f^0 \frac{D_B}{D_L} e^{-Kt}\right\} \tag{5-7}$$

and the growth law is obtained by integrating equation (5-7) to

$$x^2 = 2\Omega D_L \Delta c\left\{t + \frac{f^0 D_B}{KD_L}\left(1 - e^{-Kt}\right)\right\} \tag{5-8}$$

By analyzing the particle size of the inhibition layer as a function of the reaction time and bath temperature, the area fraction of the grain boundaries in the inhibition layer, f, was calculated. There are two assumptions made in this calculation. First, the area fraction of the two-dimensional grain boundaries represents the fraction of the total available sites within the three-dimensional layer. Second, the width of a grain boundary is approximately 1.5nm. Figure 5-4 shows the variation of f with reaction times and bath temperature.

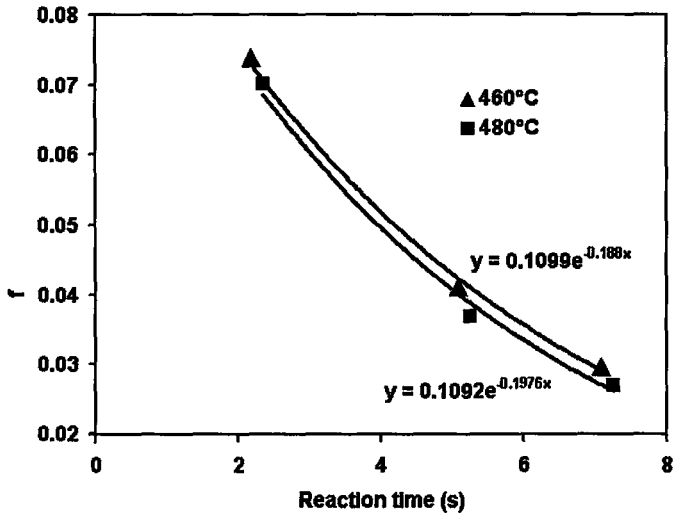

Figure 5-4: Area fraction of grain boundary varying with reaction time and bath temperature

In order to calculate the effective diffusion coefficient, the lattice and grain boundary diffusion coefficients have to be determined. From Teixeira *et al*'s experimental data [Teixeira *et al.*, 1987], it is possible to extract D_B and D_L (m^2s^{-1}) via the equations:

$$D_L = 2.2\times10^{-11}\exp\left(-\frac{0.95eV}{kT}\right) \quad (5\text{-}9)$$

$$D_B = 1.7\times10^{-12}\exp\left(-\frac{0.33eV}{kT}\right) \quad (5\text{-}10)$$

Here, k is the Boltzmann constant and T is the absolute temperature. Figure 5-5 shows the variation of the effective diffusion coefficient with the reaction time and bath temperatures based on Figure 5-4 and equations 5-9 and 5-10. From this figure, it can be seen that the microstructure of the inhibition layer has a significant influence on the diffusion rate of Fe. Thus, it indicates that the effective diffusion coefficient is not a constant but a function of reaction time and bath temperature.

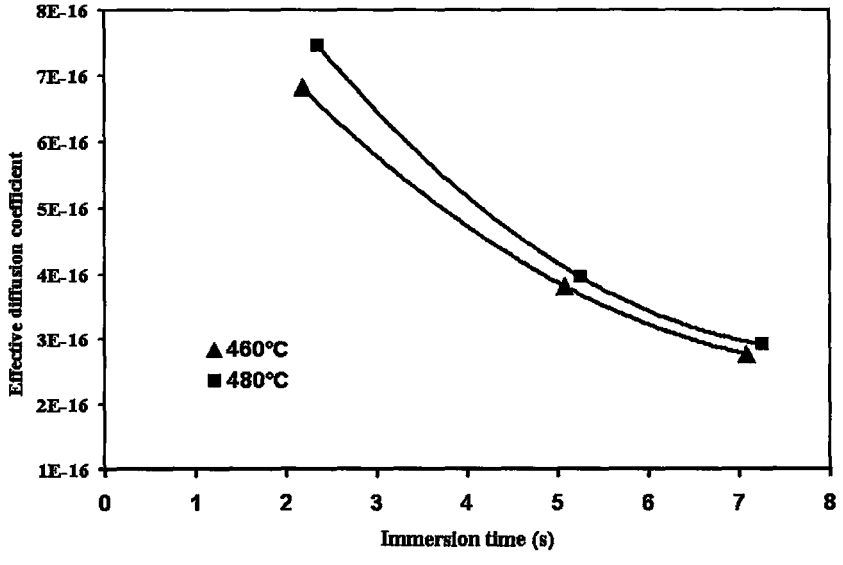

Figure 5-5: Effective diffusion coefficient as a function of reaction time and bath temperature

The thickness of the inhibition layer as a function of reaction time was calculated using equation 5-8. Table 5-2 summarizes the parameters used in these calculations for bath temperature of 460°C and 480°C. The values of these parameters were based on equations 5-4, 5-5, 5-9 and 5-10. f^0 and K were obtained by fitting the curves in Figure 5-4 with an exponential equation as shown on the figure.

Table 5-2: Values for inhibition layer growth model equation

T	t (s)	f	D_B (m^2s^{-1})	D_L (m^2s^{-1})	D_{eff} (m^2s^{-1})	f^0	K
733K (460°C)	2.186	0.074	9.15E-15	6.47E-18	6.81E-16	0.1099	0.188
	5.086	0.041			3.81E-16		
	7.086	0.030			2.77E-16		
753K (480°C)	2.354	0.070	1.05E-14	9.64E-18	7.46E-16	0.1092	0.1976
	5.254	0.037			3.96E-16		
	7.254	0.027			2.92E-16		

The modeling results with comparison to experimental data are shown in Figure 5-6. As mentioned previously, the nucleation kinetics of the Fe-Al layer reaction was not captured experimentally in the present study. According to the morphology of the inhibition layer observed for this shortest reaction time (Figure 4-7), it was found that the surface of the steel substrate was completely covered. Without better experimental evidence, the average value of Al uptake for the shortest reaction time was considered to be the initiation of diffusion controlled growth.

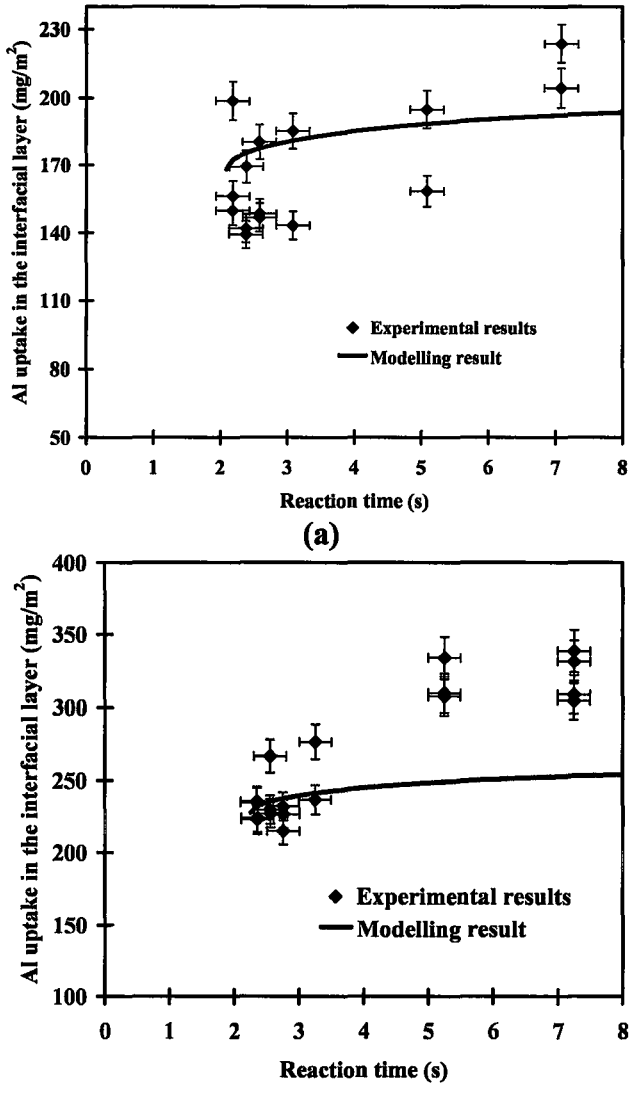

Figure 5-6: Experimental data of Al uptake of the interfacial layer as a function of reaction time for a bath with 0.2wt% dissolved Al at (a) 460°C and at (b) 480°C shown with modeling results

According to the modeling results, it was found that the increase of Al uptake with increasing reaction time was greater at 480°C than that at 460°C. This trend was consistent with experimental results concerning the influence of bath temperature on Al

uptake. It indicated that bulk diffusion played a more important role in the mixed diffusion growth mechanism at higher bath temperatures.

However, the Al uptake with reaction time based on this model seems lower than that for experimental results for both bath temperatures. In equation 5-8, the only adiustable parameters are f^0 and K when the bath temperature is fixed. These two parameters are related to the area fraction of grain boundaries. Modeling results indicated that the factor f, the area fraction of grain boundaries, was underestimated or there exists other low resistance diffusion path in the inhibition layer. There are some adjustments and modifications that could be done for future work. It has been observed that the particles of the inhibition layer vary in size and shape. However, generally speaking, these grains were close to equiaxed, especially for the particles formed at very short time and the particles formed the bottom layer in longer reaction time. Thus, so-called "triple junctions" must exist and they are also low resistance diffusion paths. However, the contribution of these triple junctions to the diffusion constant was not calculated in the present model. Thus, the existence of significant numbers of triple junctions could lead to underestimate the effective diffusion coefficient and eventually result in lower values of Al uptake in the interfacial layer during the solid diffusion growth.

In addition, the assumption in the present model that the area fraction of two-dimensional grain boundaries represents the fraction of the total available sites within the three-dimensional layer might also cause some errors. It has been shown that the microstructure

of the inhibition layer is composed of two sublayers for longer reaction times. The upper layer is a coarse, but not compact, structure with fine crystals underneath. When the area of grain boundary was determined, the contribution from the incompact upper layer and finely crystal lower layer was not considered.

It has been approximately calculated that the Al uptake would be 62 percent greater when the area of low resistance diffusion path, including grain boundary and triple junctions, was doubled. It indicates the existence of other low resistance diffusion paths, such as triple junctions, may play a very important role in inhibition layer growth. In addition, if the area fraction of the grain boundary was fixed to the value at short reaction time, Al uptake would be increased by 14 percent. This indicates that the area fraction of grain boundaries for longer reaction time was likely underestimated due to the non-compact upper layer.

The anticipated outcome for the present model was to relate the evolution of the inhibition layer microstructure to the diffusion coefficient. A more precisely defined effective diffusion coefficient is crucial to obtain the precise value of Al uptake. However, the area fraction of low resistance diffusion path is very sensitive to the structure of the inhibition layer. Thus, there is still some work required to refine the value for this parameter.

CHAPTER 6. CONCLUSIONS AND RECOMMENDATIONS

6.1 Conclusions

1. The morphology of the inhibition layer was strongly influenced by the Al content of the zinc bath. When the zinc bath contained 0.2wt% dissolved Al, the inhibition layer formed with a layered structure for all experimental temperatures and times. The lower layer was composed of small (tens of nanometers), roughly equiaxed, close-packed crystals. The upper layer consisted of larger (from 100nm to 800nm), irregular crystals. Both layers showed a preferred orientation with the <100> direction approximately normal to the substrate surface. When the zinc bath contained 0.13wt% dissolved Al, the inhibition layer was incomplete and also contained Fe-Zn intermetallic compounds, the amount of which increased with increasing reaction time and bath temperature.

2. The growth sequence of the inhibition layer formation in the zinc bath with 0.2wt% dissolved Al was (1) Fe-Al intermetallic compounds nucleated on the surface of the steel substrate and grew until the surface was completely covered with a layer of small roughly equiaxed crystals; (2) this layer grew by Al provided from the Al-bearing zinc bath and Fe from the steel substrate through a

combination of bulk and grain boundary diffusion. The rate of Fe-Al layer growth increased with bath temperature.

3. Two Fe-Al intermetallic phases were identified for the inhibition layer in the 0.2wt% Al bath using electron backscatter diffraction (EBSD): Fe_2Al_5 and $FeAl_3$. Moreover, the EBSD examination indicated that the development of the inhibition layer consisted of several steps, namely: for short reaction times, the lower layer appears to contain a larger proportion of $FeAl_3$; as the reaction proceeds, $FeAl_3$ phase gradually transforms to Fe_2Al_5 phase by a diffusion reaction to satisfy thermodynamic equilibrium between the Zn bath and α-Fe; the metastable $FeAl_3$ phase gradually disappears and the two layer structure of the Fe_2Al_5Zn interfacial layer is formed.

4. The evolution of the interfacial layer formed in the zinc bath with 0.13wt% dissolved Al, including Fe-Al and Fe-Zn intermetallic compounds, was a result of competing reactions. In the initial period, the Fe-Al reaction dominated due to high thermodynamic driving forces. Zinc diffused through the inhibition layer simultaneously, with more rapid diffusion occurring along the substrate grain boundaries. After the substrate zinc concentration reached a critical point in the substrate grain boundaries, Fe-Zn reactions dominated. The increase in interfacial Al uptake while simultaneously increasing the amount of ζ-$FeZn_{13}$ showed that there is competition between these two reactions. After exiting the zinc bath, the

Fe-Al reaction slowed due to the limited Al supply from the Zinc overlay and Fe-Zn intermetallic compounds continued to grow by consuming the Fe-Al layer.

5. The growth kinetics of the interfacial layer, i.e. influence of reaction time on the Al uptake in the interfacial layer, was investigated. The Al uptake in the interfacial layer was found to increase with increasing reaction time for all experimental bath temperatures and for both bath compositions (0.2wt% and 0.13wt% Al). Bath temperature also has an influence on Al uptake. The Al uptake increased with increasing bath temperature in a zinc bath with 0.2wt% Al. Conversely, higher temperatures corresponded to lower Al uptake when zinc bath contained 0.13wt% Al due to more rapid breakdown of the inhibition layer with increasing temperature and the resultant increase in Fe-Zn intermetallic growth.

6. A kinetic model to describe the growth kinetics of the inhibition layer in the case of 0.2wt% Al baths as a function of temperature was proposed. This model indicates that the evolution of the inhibition layer microstructure has a significant influence on the dominant diffusion path operating during the layer growth. At shorter reaction times and lower temperatures, the finely divided microstructure and higher proportion of grain boundaries resulted in grain boundary diffusion dominating growth. For longer times and higher reaction temperatures, the coarser microstructure and reduction in grain boundary area shifted the mechanism towards bulk lattice diffusion. However, the existence of significant numbers of

triple junctions and a non-compact upper layer could lead to underestimate the effective diffusion coefficient and eventually result in an underestimation of Al uptake in the interfacial layer during solid diffusion growth.

6.2 Recommendations for Further Work

1. Try to use the combined TEM and grazing angle X-ray diffraction methods to further identify the phase constitution and structure of the interfacial layer
2. Investigate the kinetics of the inhibition layer formation of steels which have different alloying elements, such as Mn and Si, to reveal the effect of these elements on inhibition layer formation

REFERENCES

Baril, E. and G. L'Esperance (1999). "Studies of the Morphology of the Al-rich Interfacial Layer Formed during the Hot-dip Galvanizing of Steel Sheet." Metallurgical and Materials Transactions A 30A(3): 681-695.

Baril, E., G. L'Esperance and E. Boutin (1998). "Effect of Process Parameters on Inhibition Breakdown Mechanisms During Hot-dip Galvannealing". Proceedings of the 4th International Conference on Zinc and Zinc Alloy Coated Steel Sheet (GALVATECH'98). The Iron and Steel Institute of Japan: 168-173.

Belisle, S. (1993). "Effect of Galvanizing Parameters on the Aluminum Content of Galvanized Coatings". The Physical Metallurgy of Zinc Coated Steel, TMS Annual Meeting. A. R. Marder, The Minerals, Metals and Materials Society: 65-74.

Belisle, S., V. Lezon and M. Gagne (1991). "The Solubility of Iron in Continuous Hot-Dip Galvanizing Baths." Journal of Phase Equilibria 12: 259-265.

Biele, P. (1995). "Determination of the Active Al and Fe Contents in the Zinc Bath and Their Influence on Alloy Layer Formation in the Hot-dip Galvanizing Process". The Use and Manufacture of Zinc and Zinc Alloy Coated Sheet Steel Products into the 21st Century (GALVATECH'95). The Iron and Steel Society: 769-775.

Chen, Z. W., R. M. Sharp and J. T. Gregory (1990 (A)). "Lattice Parameters and Interplanar Spacings of Fe_2Al_5 and Fe_2Al_5-Zn_x." Materials Forum 14: 130-136.

Chen, Z. W., R. M. Sharp and J. T. Gregory (1990 (B)). "Fe-Al-Zn Ternary Phase Diagram at 450℃." Materials Science and Technology 6: 1173-1176.

Dubois, M. (1998). "The Al Pick Up Variations on Industrial Galvanizing Sheets". Proceedings of the 4th International Conference on Zinc and Zinc Alloy Coated Steel Sheet (GALVATECH'98). The Iron and Steel Institute of Japan: 634-641.

Dubois, M. (2004). "Al content in Intermetallic & Free Zinc on Industrial Galvanizing Sheets". Proceedings of the 6th International Conference on Zinc and Zinc Aloy Coated Steel Sheet (GALVATECH'04). Association for Iron and Steel Technology: 1079-1088.

Dubois, M. and S. Feron (1993). "Al-Pick Up on Industrial Galvanizing Sheet". The Physical Metallurgy of Zinc Coated Steel. A. R. Marder, The Minerals, Metals and Materials Society: 55-64.

Ebrill, N. J. (2000). "The Influence of The Steel Substrate Entry Temperature On Wetting and Interfacial Resistance in Hot Dip Metallic Coating". PhD thesis. Department of Chemical Engineering, The University of Newcastle, Callaghan, NSW 2308, Australia

Faderl, J., W. Maschek and J. Strutzenberger (1995). "Spangel Size and Aluminum Pick-up For Hot Dip Zinc Coating". The Use and Manufacture of Zinc and Zinc Alloy Coated Sheet Steel Products into the 21st Century (GALVATECH'95). the Iron and Steel Society: 675-685.

Faderl, J., M. Pimminger and L. Schonberger (1992). "Influence of Steel Grade and Surface Topography on the Galvannealing Reaction". Galvatech '92 Conference Proceedings. 194-198.

Furdanowicz, V. and C. R. Shastry (1999). "Distribution of Aluminum in Hot-dip Galvanized Coatings." Metallurgical and Materials Transactions A 30A: 3031-3043.

Gellings, P., E. Bree and G. Gierman (1979). "Synthesis and Charactertization of Homogeneous Intermetallic Al-Zn Compounds." Z Metallkde 70: 312.

Gellings, P., G. Gierman, D. Koster and J. Kuit (1980). "Synthesis and Charactertization of Homogeneous Intermetallic Al-Zn Compounds." Z Metallkde 71: 70.

Ghuman, A. R. P. and J. I. Goldstein (1971). "Reaction Mechanisms for the Coatings Formed During the Hot Dipping of Iron in 0 to 10 Pct Al-Zn Baths at 450°C to 470°C." Metallurgical Transactions 2: 2903-2914.

Giorgi, M.-L. and J.-B. Guillot (2004). "Modeling of the Kinetics of Galvanizing Reactions". Proceedings of the 6th International Conference on Zinc and Zinc Aloy Coated Steel Sheet (GALVATECH'04). Association for Iron and Steel Technology: 703-712.

Glodstein, J. I. (2003). "Scanning Electron Microscopy and X-ray Microanalysis". Kluwer Academic/Plenum Publishers.

Guttmann, M. (1994). "Diffusive Phase Transformations In Hot Dip Galvanzining." Materials Science Forum 155-156: 527-548.

Guttmann, M., Y. Lepretre, A. Aubry, M. J. Roch, T. Moreau, P. Drillet, J. M. Mataigne and H. Baudin (1995). "Mechnisms of the Galvanizing Reaction. Influence of Ti and P Contents in Steel and of its Surface Microstructure after Annealing". The Use and Manufacture of Zinc and Zinc Alloy Coated Sheet Steel Products into the 21st Century (GALVATECH'95). the Iron and Steel Society: 295-307.

Harvey, G. J. and P. D. Mercer (1973). "Aluminum-rich Alloy Layers Formed During the Hot-dip Galvanizing of Low Carbon Steel." Metallurgical Transactions 4: 619-621.

Herchl, R., N. N. Khoi, T. Homma and W. W. Smeltzer (1972). "Short-circuit Diffusion in the Growth of Nickel Oxide Scales on Nickel Crystal Faces." Oxidation of Metals 435-46.

Hertveldet, I., J. Craenen, J. Dilewijns, B.Blanpain, C. Xhoffer and B. C. D. Cooman (1998). "The Structure of the Inhibition layer after Hot-dip Galvanizing of Ti IF-DDQ, TiNb IF-DDQ and TiNb+P IF-HSS Substrates". Zinc-Based Steel Coating Systems: Production and Performance, TMS Annual Meeting. The Minerals, Metals and Materials Society: 13-25.

Hisamatsu, Y. (1989). "Science and Technology of Zinc and Zinc Alloyed Coated Steel Sheet". Galvatech '89 Conderence Proceedings. 3-12.

HKL-Technology (2006). "Operator's EBSD Trainning Course."

Inagaki, J., M. Sakurai and M. Sagiyama (1995). "Alloying Reactions in Hot-Dip Galvanizing and Galvannealing Process." ISIJ International 35: 1388.

Isobe, M. (1992). "Initial Alloy Behaviour in Galvannealing Process." CAMP-ISIJ **5**: 1629-1632.

Jordan, C. E. and A. R. Marder (1997 (A)). "Fe-Zn Phase Formation in Interstitial-free Steels Hot-Dip Galvanized at 450℃, Part Ⅰ 0.00wt% Al-Zn Baths." Journal of Materials Science 32: 5593-5602.

Jordan, C. E. and A. R. Marder (1998). "Inhibition layer breakdown and outburst Fe-Zn alloy formation during galvanizing". Zinc-Based Steel Coating Systems: Production and Performance, TMS Annual Meeting. The Minerals, Metals and Materials Society: 115-126.

Jordan, C. E., R. Zuhr and A. R. Marder (1997 (B)). "Effect of Phosphorous Surface Segregation on Iron-Zinc Reaction Kinetics during Ho-dip Galvanizing." Metallurgical and Materials Transactions A 28A: 2695-2703.

Jordan, D. E. and A. R. Marder (1995). "Alloy Layer Growth During Hot-dip Galvanizing at 450°C". The Use and Manufacture of Zinc and Zinc Alloy Coated Sheet Steel Products into the 21st Century (GALVATECH'95). the Iron and Steel Society: 319-325.

Kaye, M. H., W. T. Thompson and J. R. McDermid (2005). "The Zn-rich Corner of the Zn-Al-Fe Phase Diagram for Use in Continuous Galvanizing." Materials Science & Technology Conference 2005, Developments in Sheet Products for Automotive Applications: 199-210.

Kiusalaas, R., G. Engberg, H. Klang, E. Schedin and L. Schon (1989). "Control of Texture and Formation of Intermetallic Phases in Continuously Hot-Dip Galvanizing Coatings." Galvatech '89 Conderence Proceedings: 485.

Kofstad, P. (1988). "High Temperature Corrosion". Elsevier Applied Science Publishers Ltd.

Lepretre, Y. and J. M. Mataigne (1998 (A)). "Reaction Mechanisms During Hot-dip Galvanizing: Effect of Phosphorous on Coating Development". Proceedings of the 4th

International Conference on Zinc and Zinc Alloy Coated Steel Sheet (GALVATECH'98). The Iron and Steel Institute of Japan: 133-140.

Lepretre, Y., J. M. Mataigne, M. Guttmann and J. Philibert (1998 (B)). "Reactive Interfiffusion in the Fe-Al-Zn System: Reaction Mechanisms during Hot-dip Galvanizing." Zinc-Based Steel Coating Systems: Production and Performance: 95-114.

Lepretre, Y., J. M. Mataigne, M. Guttmann and J. Philibert (1998 (B)). "Reactive Interdiffusion in the Fe-Al-Zn System: Reaction Mechanisms during Hot-dip Galvanizing." Zinc-Based Steel Coating Systems: Production and Performance, TMS Annual Meeting: 95-114.

Lin, C. S. and M. Meshii (1995 (A)). "Effect of Steel Chemistry on the Formation of the Alloy Layers on the Commercial Hot-dip Coatings". The Use and Manufacture of Zinc and Zinc Alloy Coated Sheet Steel Products into the 21st Century (GALVATECH'95). the Iron and Steel Society: 335-341.

Lin, C. S., M. Meshii and C. C. Cheng (1995 (B)). "Phase Evolution During Galvanneal Process". The Use and Manufacture of Zinc and Zinc Alloy Coated Sheet Steel Products into the 21st Century (GALVATECH'95). the Iron and Steel Society: 485-495.

Marder, A. R. (2000). "The Metallurgy of Zinc-coated Steel." Progress in Materials Science 45(3): 191-271.

McDermid, J. and C. E. Dewey (2002 (A)). "Optimizing the GA to GI Transition at Pro-Tec CGL #1". Proceedings of the 92 Galvanizers Association Meeting. Noranda Incorporation:

McDermid, J. R., E. Baril and F. E. Goodwin (2004 (A)). "Galvanizing Bath Management during Galvanize to Galvanneal and Galvanneal to Galvanize Product Transitions". Proceedings of the 6th International Conference on Zinc and Zinc Aloy Coated Steel Sheet (GALVATECH'04). Association for Iron and Steel Technology: 855-869.

McDermid, J. R., E. Baril and W. T. Thompson (2004 (B)). "Fe Solubility in the Zn-Al-Fe System for Use in Continuous Galvanizing and Galvanealing". Proceedings of the 6th International Conference on Zinc and Zinc Aloy Coated Steel Sheet (GALVATECH'04). Association for Iron and Steel Technology: 491-499.

McDermid, J. R. and W. T. Thompson (2002 (B)). "Fe Solubility in the Zn-rich Corner of the Zn-Al-Fe System for Use in Continuous Galvanizing." 44th Mechanical Working and Steel Processing Conference Proceedings 805-813.

McDevitt, E., Y. Morimoto and M. Meshii (1997). "Characterization of the Fe-Al Interfacial Layer in a Commercial Hot-dip Galvanized Coating." ISIJ International 37(8): 776-782.

McDevitt, E. T. and M. Meshii (1998). "Electron Microscopy Study of the Microstructural Evolution in the Early Stages of Galvannealing". Zinc-Based Steel Coating Systems: Production and Performance, TMS Annual Meeting. The Minerals, Metals and Materials Society: 127-136.

Morimoto, Y., E. Mcdevitt and M. Meshii (1997). "Characterization of the Fe-Al Inhibition Layer Formed in the Initial Stages of Hot-dip Galvannealing." ISIJ International 37(9): 906-913.

Nakano, J. (2006). "A computational thermodynamic study of the systems Zn-Fe and Zn-Fe-Al". PhD Thesis. Materials Science and Engineering, McMaster University, Hamilton, Ontaril, Canada

Noranda, Technology Center. "Zinc Products and Applications: Galvanized Coatings Selective Stripping Procedure."

Perrot, P., J.-C. Tissier and J.-Y. Dauphin (1992). "Stable and Metastable Equilibria in the Fe-Zn-Al System at 450℃." Z Metallkde 83: 786-790.

Perrow, J. M., W. W. Smeltzer and J. D. Embury (1968). "The Role of Structureal Defects in the Growth of Nickel Oxide Films." ACTA Metallurgica 16: 1209-1218.

Perrow, J. M., W. W. Smeltzer and R. K. Ham (1967). "On the Nature of Short-circuit Diffusion Paths in Nickel Oxide Films." ACTA Metallurgica 15: 577-579.

Philibert, J. (1994). "Reactive Interdiffusion." Materials Science Forum 155-156: 15-30.

Porter, D. A. and K. E. Easterling (1992). "Phase Transformations in Metals and Alloys". Nelson Thornes Ltd.

Price, S. E., V. Randle and M. Pichilingi (1999). "Study of Aluminium Inhibition Layer Formed during Hot-dip Stage of Galvannealing on Titanium Interstitial Free and Rephosphorised Titanium Interstitial Free Substrates." Ironmaking and Steelmaking 26(5): 378-386.

Proskurkin, E. V. and N. S. Gorbunov (1975). "Galvanizing Sherardizing and Other Zinc Diffusion Coatings".

Saito, M., Y. Uchida, T. Hirose and Y. Hisamateu (1991). "Formation Behaviour of Alloy Layer in Initial Stages of Galvanizing." J. ISIJ 77: 947-954.

Smeltzer, W. W., R. R. Haering and J. S. Kirkaldy (1961). "Oxidation of Metals by Short Circuit and Lattice Diffusion of Oxygen." ACTA Metallurgica 6: 880-885.

Tang, N. (1995 (A)). "Modeling Al Enrichment in Galvanized Coatings." Metallurgical and Materials Transactions A 26A: 1699-1704.

Tang, N. (1996). "450℃ Isothermal of Zn-Fe-Al Phase Diagram Update." Journal of Phase Equilibria 17: 396-398.

Tang, N. (1998 (A)). "Thermodynamics and Kinetics of Alloy Formation in Galvanized Coatings". Zinc-Based Steel Coating Systems: Production and Performance, TMS Annual Meeting. The Minerals, Metals and Materials Society: 3-12.

Tang, N. (1998 (B)). "Predicting Aluminum Level of Continuous Galvanizing Baths". Proceedings of the 4th International Conference on Zinc and Zinc Alloy Coated Steel Sheet (GALVATECH'98). The Iron and Steel Institute of Japan: 654-658.

Tang, N. (1999). "Characteristics of Continuous Galvanizing Baths." Metallurgical and Materials Transactions B 30B: 144-148.

Tang, N. (2000). "Determination of Liquid-Phase Boundaries in the Zn-Fe-Mx Systems." Journal of Phase Equilibria 21(1): 70-77.

Tang, N. and G. R. Adams (1993). "Studies on the Inhibition of Alloy Formation in Hot-dip Galvanized Coatings". The Physical Metallurgy of Zinc Coated Steel. A. R. Marder, The Minerals, Metals and Materials Society: 41-54.

Tang, N., G. R. Adams and P. S. Kolisnyk (1995 (B)). "On Determining Effective Aluminum in Continuous Galvanizing Baths". The Use and Manufacture of Zinc and Zinc Alloy Coated Sheet Steel Products into the 21st Century (GALVATECH'95). the Iron and Steel Society: 777-782.

Teixeira, S. R., P. H. Dionisio, E. F. D. Silveira, F. L. F. Jr, W. H. Schreiner and I. J. R. Baumvol (1987). "Interdiffusion and Reaction in the Fe-Al Bilayer Ⅰ : Rutherford Backscattering Analysis of Furnace-annealed Samples." Materials Science & Engineering 96: 267-277.

Toussaint, P., L. Segers, R. Winand and M. Dubois (1998 (A)). "Short time Investigation of Hot Dip Galvanizing of Steel under Controlled Hydrodynamics." Galvatech '98 Conderence Proceedings: 141-146.

Toussaint, P., L. Segers, R. Winand and M. Dubois (1998 (A)). "Short time Investigation of Hot Dip Galvanizing of Steel under Controlled Hydrodynamics". Proceedings of the 4th International Conference on Zinc and Zinc Alloy Coated Steel Sheet (GALVATECH'98). The Iron and Steel Institute of Japan: 141-146.

Toussaint, P., L. Segers, R. Winand and M. Dubois (1998 (B)). "Study and Modelling of Interfacial Al Take-up in Continuous Galvanizing using a Lab Simulator". Zinc-Based Steel Coating Systems: Production and Performance, TMS Annual Meeting. The Minerals, Metals and Materials Society: 27-37.

Toussaint, P., L. Segers, R. Winand and M. Dubois (1998 (C)). "Mathematical Modelling of Al Take-up during the Interfacial Inhibiting Layer Formation in Continuous Galvanizing." ISIJ International 38(9): 985-990.

Winand, R., L. Segers and P. Toussaint (1997). "Nature of Aluminum Pick-up on Steel Strip at Short Immersion Times." International Lead Zinc Research Organization (ILZRO) Project.

Yamaguchi, H. and Y. Hisamatsu (1979). "Reaction Mechanism of the Sheet Galvanizing." Transactions of the Iron and Steel Institute of Japan 19(11): 649-658.